



Invited review article

The Cascadia Paradox: Mantle flow and slab fragmentation in the Cascadia subduction system



Maureen D. Long

Department of Geology and Geophysics, Yale University, New Haven, CT, USA

ARTICLE INFO

Article history:

Received 20 July 2016

Received in revised form

30 September 2016

Accepted 30 September 2016

Available online 11 October 2016

Keywords:

Subduction

Mantle flow

Seismic anisotropy

Mantle dynamics

Cascadia

Pacific northwest

ABSTRACT

The pattern of mantle flow in subduction systems and the processes that control the mantle flow field represent fundamental but still poorly understood aspects of subduction dynamics. The Cascadia subduction zone is a compelling system in which to understand the controls on mantle flow, especially given the dense geophysical observations recently provided by EarthScope, GeoPRISMS, the Cascadia Initiative, and related efforts. Observations of seismic anisotropy, which provide relatively direct constraints on mantle flow, are particularly intriguing in Cascadia because they seem to yield contradictory views of the mantle flow field in different parts of the system. Specifically, observations of seismic anisotropy on the overriding plate, notably in the central portion of the backarc, apparently require a significant component of three-dimensional, toroidal flow around the slab edge. In contrast, new observations from offshore stations are compellingly explained with a simple two-dimensional entrained flow model. Recent evidence from seismic tomography for the likely fragmentation of the Cascadia slab at depth provides a further puzzle: how does a fragmented slab provide a driving force for either two-dimensional entrained flow or three-dimensional toroidal flow due to slab rollback? Resolution of this apparent paradox will require new imaging strategies as well as the integration of constraints from seismology, geodynamics, and geochemistry.

© 2016 Elsevier Ltd. All rights reserved.

Contents

1. Introduction	151
2. Observations of seismic anisotropy	154
2.1. Shear wave splitting: methodology and interpretation	154
2.2. Shear wave splitting results: onshore	154
2.3. Shear wave splitting results: offshore	157
2.4. Other observations: surface waves, receiver functions, and anisotropy tomography	158
3. Observations of volcanism and geochemistry	159
4. Geodynamic modeling constraints	161
5. Possible fragmentation of the Juan de Fuca slab at depth	163
6. The Cascadia Paradox: where do we stand?	164
7. Conclusions	167
Acknowledgements	167
References	167

1. Introduction

The Cascadia subduction zone (Fig. 1), where the Juan de Fuca, Gorda, and Explorer Plates sink beneath North America, is impor-

tant to our understanding of subduction systems for a host of reasons, including the documented occurrence of magnitude ~9 megathrust earthquakes in the recent past (e.g., Goldfinger et al., 2003; Wang and Tréhu, 2016). The Juan de Fuca, Gorda, and Explorer Plates are remnants of the Farallon Plate, which has experienced subduction beneath North America for the past ~150 Ma (e.g., Severinghaus and Atwater, 1990). In many ways Cascadia can be considered as an endmember system among subduction zones

E-mail address: Longmaureen.long@yale.edu

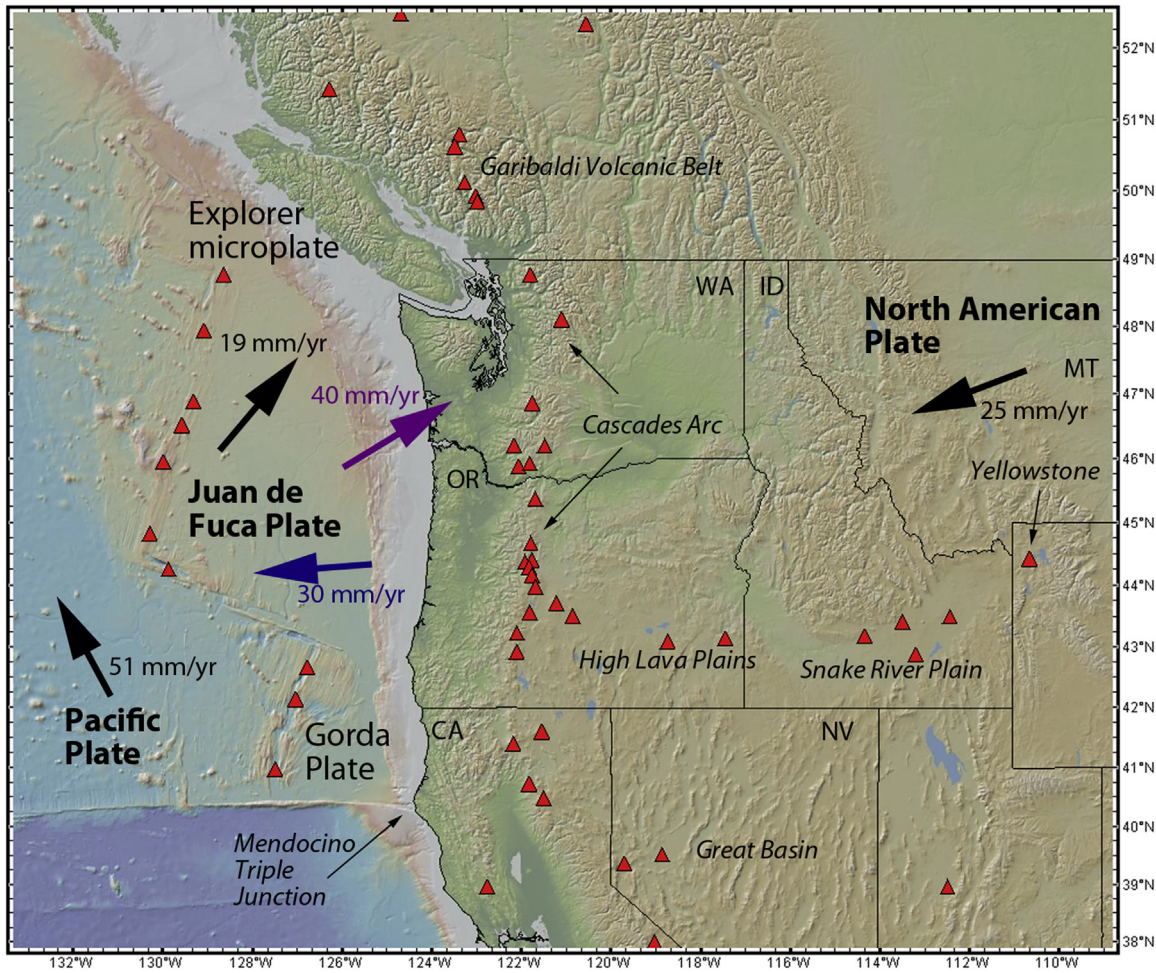


Fig. 1. General tectonic setting and geographic features of the Cascadia subduction zone. Background colors show bathymetry (offshore) and topography (onshore); Holocene volcanoes are marked with red triangles. Thin black lines show the outlines of US states (Washington, Oregon, California, Idaho, Montana, and Nevada are marked with two-letter abbreviations), and major geographic features referred to in the text are marked in italics. The Pacific, North American, Juan de Fuca, and Gorda Plates are marked, along with the Explorer microplate. Thick black arrows show absolute motion of the major plates in a hotspot reference frame, thick purple arrow shows the relative motion (convergence direction) between the Juan de Fuca and North American plates, and thick blue arrow shows the motion of the Juan de Fuca trench in a hotspot reference frame, from Schellart et al. (2008). Plate motion directions and rates (shown) were calculated using the UNAVCO plate motion calculator (<https://www.unavco.org/dxdt/model>).

globally, as it involves the subduction of a particularly young, warm, and presumably weak plate (e.g., Heuret and Lallemand, 2005) that is also relatively narrow in along-strike extent (~1400 km) compared to the global population of subduction zones (e.g., Schellart et al., 2010). The Cascadia subduction system also exhibits interesting kinematics, with significant present-day trench migration and slab rollback (~35 mm/yr in a Pacific hotspot reference frame) (Schellart et al., 2008) and crustal block rotation on the overriding plate (e.g., McCaffrey et al., 2007). The subduction zone has exhibited complex and poorly understood patterns of volcanism in the backarc over the past ~17 Ma (Fig. 2), including the eruptions of the Steens/Columbia River flood basalts (S/CRB) (e.g., Geist and Richards, 1993; Camp and Ross, 2004) and subsequent bimodal and partially time-progressive volcanism in the High Lava Plains (HLP) and Snake River Plain (SRP) (e.g., Leeman and Annen, 2008; Ford et al., 2013). Cascadia is well instrumented geophysically, particularly with recent data collection efforts associated with the USArray and Plate Boundary Observatory components of the EarthScope program, the combined onshore/offshore Cascadia Initiative passive seismic experiment, and its selection as a GeoPRISMS primary site. Despite the relative wealth of observational constraints, however, key aspects of Cascadia subduction zone behavior remain elusive. Among the most fundamental of

these is the pattern of mantle flow in the subduction system, which remains poorly understood despite extensive study.

The observation of the directional dependence of seismic wave speeds yields perhaps the most direct constraints available on patterns of deformation in the Earth's mantle, including both present-day flow in the asthenosphere and past deformation in the lithosphere. In the upper mantle, seismic anisotropy is thought to be mainly controlled by the crystallographic preferred orientation (CPO) of olivine, the primary constituent mineral (e.g., Karato et al., 2008). When a volume of mantle rock is subjected to strain in the dislocation creep regime, individual grains rotate into preferred orientations, leading to a bulk seismic anisotropy over length scales relevant to seismic wave propagation. The relationships between strain and the resulting seismic anisotropy are complex and depend on the conditions of deformation, such as stress, temperature, pressure, volatile content, and amount of strain (e.g., Karato et al., 2008; Skemer and Hansen, 2016). Furthermore, CPO of a mantle rock reflects the accumulation of strain over what may be a complex deformation history, particularly in a complicated flow regime in which the geometry of deformation may change rapidly in space and/or time (e.g., Boneh et al., 2015). Despite the potential complications, seismologists often use a set of simplified relationships between the geometry of anisotropy and the likely strain direction

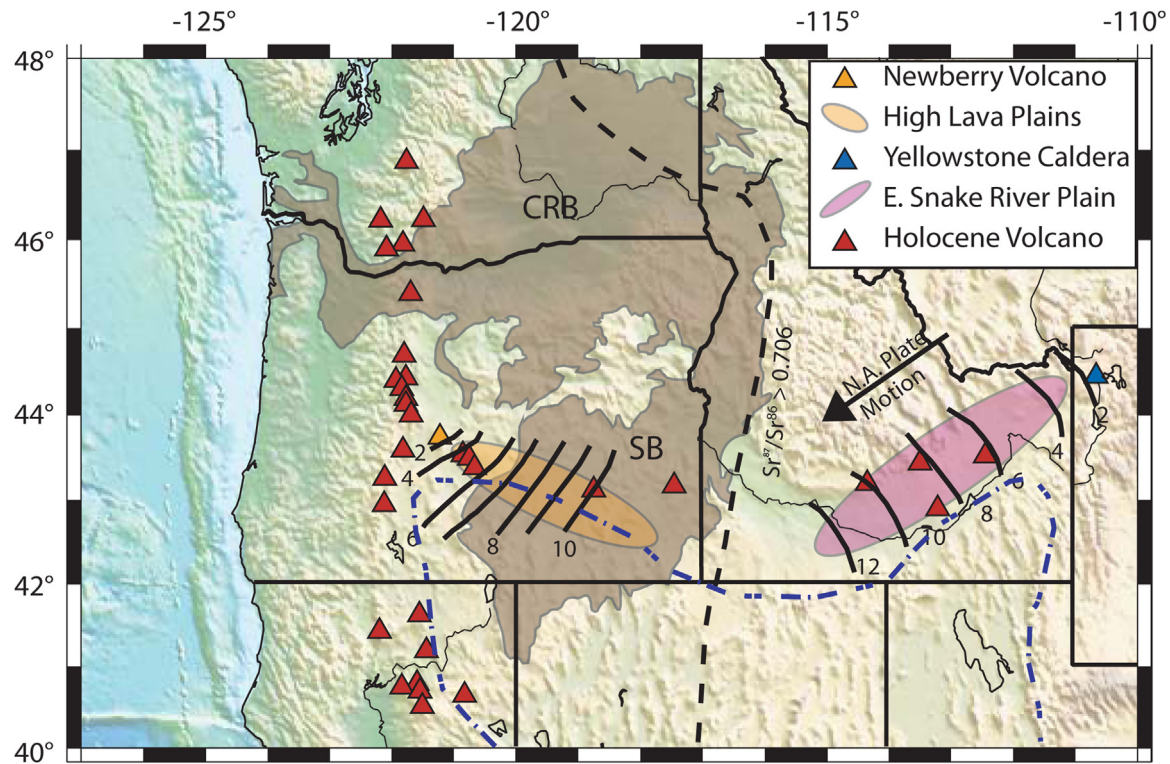


Fig. 2. Map of volcanic features of the central Cascadia arc and backarc, lightly modified from Long et al. (2009). Black contours indicate the approximate age progression (in Ma) of rhyolitic volcanism in the High Lava Plains (yellow) and the Snake River Plain (pink). Black dashed line shows the approximate location of the edge of cratonic North America, based on the $\text{Sr}^{87}/\text{Sr}^{86} = 0.706$ line. Blue dashed line shows the approximate northern limits of Basin and Range extension. Brown highlighted area indicates region covered by Miocene flood basalts, including the Columbia River basalts (CRB) to the north and the Steens basalts (SB) to the south. Red triangles indicate locations of Holocene volcanism. Newberry Volcano is marked with an orange triangle; Yellowstone Caldera is marked with a blue triangle. Details of underlying data are given in Long et al. (2009).

to interpret seismic anisotropy measurements in terms of mantle flow (e.g., Long and Becker, 2010).

Measurements of seismic anisotropy in subduction zone settings are particularly intriguing (if also notably challenging to interpret) because they can shed light on the pattern of mantle flow in subduction systems. The classical model for such flow (Fig. 3) is two-dimensional, with corner flow above the slab and entrained flow beneath; however, observations of seismic anisotropy in subduction systems often deviate from the predictions of simple two-dimensional flow in combination with the simplest olivine fabric scenarios (for a recent review, see Long, 2013). To first order, the entrained flow scenario would generally predict fast directions of wave propagation that are parallel to plate motion (that is, to the convergence direction, or generally perpendicular to the trench for many subduction systems), although deviations from this prediction could result from the presence of unusual olivine fabrics (e.g., Kneller et al., 2005), strong radial anisotropy in the subslab mantle (Song and Kawakatsu, 2012), or the presence of a dipping axis of anisotropic symmetry (e.g., Levin et al., 2007a). Another endmember scenario for flow in subduction systems (Fig. 3) invokes the presence of dominantly toroidal flow (that is, three-dimensional flow with a significant component of trench-parallel motion) induced by the motion of the trench itself in a mantle reference frame. This type of flow field, first suggested on the basis of seismic anisotropy observations by Russo and Silver (1994), has been observed in laboratory and numerical models that include slab rollback (e.g., Buttes and Olson, 1998; Schellart et al., 2007; Druken et al., 2011; Faccenda and Capitanio, 2013; Paczkowski et al., 2014). Toroidal flow has been invoked to explain several aspects of commonly observed (though not ubiquitous) anisotropy patterns in subduction systems. These include domi-

nantly trench-parallel fast directions both beneath the slab (e.g., Russo and Silver, 1994; Long and Silver, 2009; Lynner and Long, 2014) and in the mantle wedge (e.g., Hoernle et al., 2008; Long et al., 2016), as well as patterns of anisotropy on the overriding plate that are consistent with toroidal flow, particularly around the slab edge (e.g., Peyton et al., 2001).

Interestingly, both endmember mantle flow scenarios (two-dimensional entrained flow and three-dimensional toroidal flow) are commonly invoked to explain observed patterns of seismic anisotropy in the Cascadia subduction system. For example, global compilations of shear wave splitting in subduction zones (Long and Silver, 2008, 2009) have highlighted the fact that Cascadia exhibits dominantly plate motion parallel fast splitting directions for SKS phases measured at stations close to the trench, as expected for two-dimensional entrained flow beneath the slab, and consistent with the interpretation of many previous studies in Cascadia. This view has been bolstered by recent observations of seismic anisotropy on the downgoing plate, which generally seem to be consistent with the idea of two-dimensional, plate-driven flow beneath the Juan de Fuca slab (Bodmer et al., 2015; Martin-Short et al., 2015). However, the three-dimensional toroidal flow model has also been widely invoked for Cascadia, most notably by Zandt and Humphreys (2008), who argued that patterns of shear wave splitting in the western US (as imaged before the advent of EarthScope USArray data) correspond to the flow vectors predicted by laboratory experiments that include slab rollback (Piromallo et al., 2006). Of course, two-dimensional entrained flow and three-dimensional toroidal flow represent conceptual end-member scenarios, and the actual flow field may well involve a combination of both types (for example, large-scale 3D toroidal flow can coexist with a layer of entrained flow directly beneath the

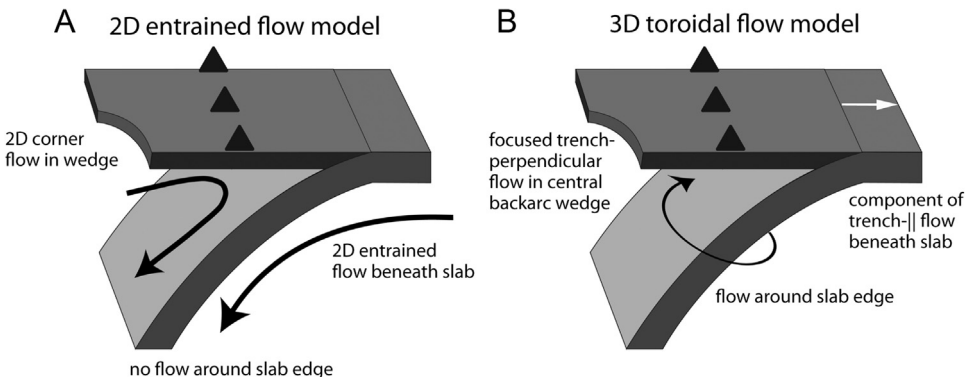


Fig. 3. Cartoon sketch of two simplified endmember models for subduction zone mantle flow: the 2D entrained flow model (a) and the 3D toroidal flow model (b). In (a), viscous coupling between the downgoing slab and the surrounding mantle leads to 2D corner flow in the mantle wedge and 2D entrained flow beneath the slab (black arrows). Black triangles on the overriding plate indicate arc volcanoes. In (b), the migration of the trench (white arrow) and rollback of the slab induces a 3D flow field (black arrow), in which flow is deflected horizontally around the slab edge, leading to a significant component of trench-parallel flow beneath the slab and focused flow parallel to trench migration (that is, generally perpendicular to the trench) in the central portion of the wedge backarc. These sketches indicate highly simplified endmember models; the actual flow field in any given subduction system likely reflects a combination of the two.

slab; e.g., [Martin-Short et al., 2015](#)). However, it is clear from the abundant literature on seismic anisotropy observations in the Cascadia subduction zone that there is as yet no consensus on which model (or combination of models) can best explain the data, and both endmember scenarios are commonly invoked.

Despite the lack of consensus, understanding the pattern of mantle flow in the Cascadia subduction zone is an important scientific challenge. Mantle flow affects a host of crucial subduction zone processes, from the generation of melt and volcanism in the arc and backarc to the evolution of the slab morphology. Understanding how the mantle flow field interacts with aspects of the Cascadia subduction zone, including its striking backarc volcanism and overriding plate kinematics and the geometry of the possibly fragmented slab at depth, is key to understanding the system's dynamics. More generally, because Cascadia is an endmember subduction system in many ways, understanding its behavior is needed to establish a baseline for the behavior of subduction zones globally, particularly those that involve a young slab. Cascadia is much better instrumented geophysically than most subduction zones worldwide and has the advantage of extensive offshore instrumentation on the downgoing plate due to the recent Cascadia Initiative ([Toomey et al., 2014](#)). Here I review observations of seismic anisotropy and slab morphology in the Cascadia subduction system, along with constraints from geochemistry, volcanism, and geodynamic modeling, and discuss the apparent paradox in their interpretation.

2. Observations of seismic anisotropy

2.1. Shear wave splitting: methodology and interpretation

Shear wave splitting or birefringence ([Fig. 4](#)) is a commonly studied manifestation of anisotropy in the seismic wavefield (e.g., [Silver, 1996](#); [Savage, 1999](#)). Briefly, shear wave splitting refers to the partitioning of shear wave energy into two quasi-S waves with different wavespeeds; the polarizations of the fast and slow quasi-S waves are controlled by the geometry of anisotropy. As the two quasi-S waves propagate at different speeds, they accumulate a time delay that reflects a combination of the strength of anisotropy and the thickness of the anisotropic layer. Analysis involves the measurement of the orientation of the fast shear arrival, ϕ , and the delay time, δt , directly from the seismogram. A variety of seismic phases can be used for shear wave splitting analysis, commonly including core phases such as SKS and (in subduction zones) local S phases from earthquakes within the subducting slab itself.

The interpretation of fast orientation in terms of mantle flow direction in a complex tectonic setting such as a subduction zone is not straightforward (e.g., [Long, 2013](#)). For the simple case of horizontal flow with a vertical gradient in flow velocity (that is, simple shear with a horizontal shear plane), the formation of A-, C-, or E-type olivine fabric (e.g., [Zhang and Karato, 1995](#); [Karato et al., 2008](#)) would result in a fast splitting orientation that is parallel to the shear direction. Therefore, the idea that ϕ generally corresponds to the direction of mantle flow is a commonly used guideline in the shear wave splitting literature. However, this relationship can be complicated by the presence of B-type olivine fabric, which changes by 90° the relationship between strain and the fast splitting direction and which requires high stress, low temperature, and the presence of water (e.g., [Jung and Karato, 2001](#); [Jung et al., 2006](#)). A simple dependence of fast splitting orientation on flow geometry can also be complicated by the presence of hydrous phases (e.g., [Katayama et al., 2009](#); [Jung, 2011](#)) or complex deformation that varies rapidly in space and/or time (e.g., [Boneh et al., 2015](#)). For much of the Cascadia subduction zone, it is likely that A-, C-, or E-type olivine fabric is present, given the relatively high temperatures, with the exception of the cold corner of the forearc mantle wedge, where serpentinization is likely (e.g., [Bostock et al., 2002](#); [Wagner et al., 2013](#)). Therefore, beneath Cascadia the common interpretation that ϕ generally corresponds to the horizontal mantle flow direction is usually applied; however, deviations from this simple relationship are certainly possible.

2.2. Shear wave splitting results: onshore

Shear wave splitting has been extensively studied within the central and southern portion of the Cascadia subduction zone using stations located on the overriding plate. The deployment of the USArray TA stations in the Pacific Northwest (PNW) between roughly 2006–2009 resulted in much denser station coverage than had been available previously (a general overview of shear wave splitting patterns throughout the western US is given by [Liu et al., 2014](#)). While a few studies of local S splitting from relatively shallow slab earthquakes in Cascadia have been published (e.g., [Currie et al., 2001](#); [Balfour et al., 2012](#); [Bostock and Christensen, 2012](#)), they mostly reflect anisotropy in the crust of the overriding plate rather than upper mantle anisotropy, and the delay times for local S phases are typically much smaller than for SKS phases (on the order of ~ 0.1 s, rather than $\sim 1\text{--}2$ s for SKS).

Large-scale patterns in SKS splitting parameters for the PNW and surrounding region are well illustrated by compilations of mea-

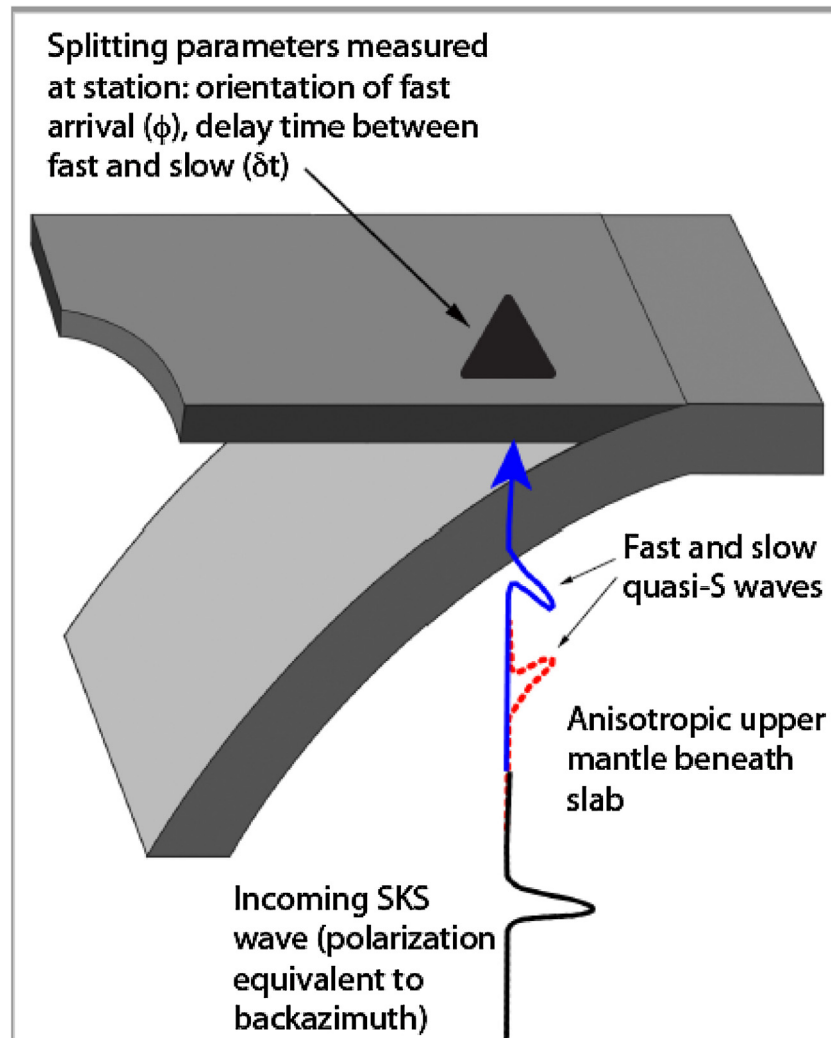


Fig. 4. Sketch of the splitting of a vertically propagating SKS phase into fast (solid blue) and slow (dotted red) quasi-S waves, after image by Crampin (1981), in a subduction zone setting. In this example there is an anisotropic region in the upper mantle beneath the subducting slab. SKS splitting measurements involve the determination of the orientation of the fast quasi-S wave, ϕ , and the delay time between the fast and slow arrivals, δt , from an individual seismogram. Note that for a realistic upper mantle anisotropy scenario, delay times (~1–2 s) are generally smaller than the period of the wave (~10 s for SKS), so the fast and slow quasi-S arrivals will not be completely separated in practice.

surements for TA (and other) stations, such as those of Fouch and West (2008), West et al. (2009), and Liu et al. (2014). To illustrate these large-scale patterns, Fig. 5 shows spatially smoothed average splitting parameters from Liu et al. (2014), which includes both the TA and stations from other networks. Stations located in the Cascades arc and forearc region exhibit fast orientations which are generally oriented ENE–WSW, roughly parallel to the direction of convergence between the Juan de Fuca and North American plates, although at stations in Washington the fast directions trend slightly more E–W. There is a noticeable departure from this pattern, however, in the vicinity of the Mendocino triple junction. There are along-strike variations in measured δt values in the arc and forearc, which generally range between ~1–1.8 s and which are highest beneath Oregon. Moving into the Cascades backarc region of eastern Washington, Oregon, and Nevada, there is a pronounced rotation to more nearly E–W fast directions, with notably high delay times beneath southeastern Oregon and southwestern Idaho. To the south, beneath the Great Basin of Nevada, there is a nearly circular (or arcuate) pattern of ϕ , with generally smaller delay times. Moving further east to stations that overlie the cratonic portion of North America, fast directions at stations in western Idaho and eastern Montana are generally NE–SW and are nearly parallel to

the APM of the North American plate, while stations to the south exhibit more complexity.

These overall patterns are generally thought to reflect regional variations in the factors controlling upper mantle anisotropy and flow, with a transition from flow that is controlled by the subduction of the Cascadia slab at stations in the forearc, arc, and backarc region, to flow that is controlled more by absolute plate motion (APM), lithospheric anisotropy, and/or a combination of these and other factors at stations located further to the east. Many of these large-scale features have been characterized in detail by individual studies. For example, observations of SKS fast splitting directions that are generally parallel to the convergence direction between the Juan de Fuca and North American plates at stations located in and around the Cascadia forearc region were documented by Currie et al. (2004), who focused on stations located in Washington and southern Vancouver Island, Canada. In western Canada more generally, studies have found evidence for convergence-parallel ϕ (e.g. Bostock and Cassidy, 1995; Evans et al., 2006), but the station coverage is generally sparse. SKS splitting measurements at stations of a dense broadband array deployed across the forearc, arc, and backarc region in central Oregon in the early 1990s also yield evidence for convergence-parallel ϕ in the forearc and arc regions,

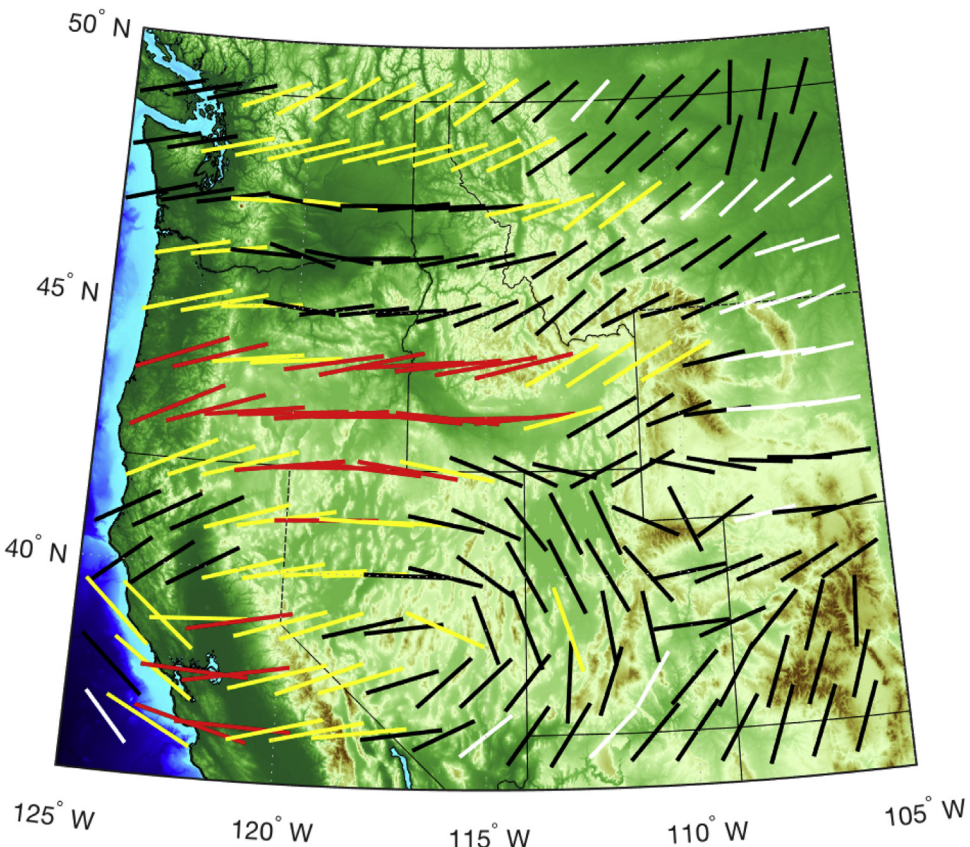


Fig. 5. Spatially averaged shear wave splitting parameters for the Pacific Northwest and surrounding region, from the database of Liu et al. (2014). Individual measurements were averaged at their piercing points at depth = 200 km in overlapping circles of radius = 1° (for details, see Liu et al., 2014). The resulting smoothed spatial distribution of splitting parameters shows systematic variations. Bars are oriented in the fast splitting direction and scaled and colored by delay time, with red bars indicating average $\delta t > 1.6$ s, yellow bars indicating $1.6 \text{ s} > \delta t > 1.3$ s, black bars indicating $1.3 \text{ s} > \delta t > 1.0$ s, and white bars indicating $\delta t < 1.0$ s.

with a rotation to generally E-W fast directions in the backarc (Fabritius, 1995; Fouch and West, 2008; see also Xue and Allen, 2006 and Long et al., 2012). Finally, measurements by Eakin et al. (2010) at stations located in the forearc region of Oregon and Washington also show clear evidence for fast directions parallel to the subduction direction.

The High Lava Plains (HLP) region of eastern Oregon, located in the backarc of the Cascadia subduction system, has been extensively studied due to its striking volcanic activity over the past ~12 Ma (e.g., Ford et al., 2013). SKS splitting measurements from two temporary deployments of broadband seismometers (the OATS deployment in 2003–2006 and the HLP experiment in 2006–2009) reveal strong SKS splitting with individual delay times reaching ~2.5 s and dominantly E-W fast directions (Xue and Allen, 2006; Long et al., 2009). Importantly, the fast directions are not parallel to either the absolute motion of the North American plate or the subduction convergence direction at the trench; instead, the fast directions are parallel to the motion of the Juan de Fuca trench, which is rolling back to the west as the overriding plate undergoes modest extension (e.g., Druken et al., 2011).

Beneath the Snake River Plain region in Idaho and the region surrounding Yellowstone, a number of regional studies have examined the pattern of SKS splitting (e.g., Schutt et al., 1998; Walker et al., 2004; Waite et al., 2005). The SRP exhibits a trend of age-progressive rhyolitic volcanism parallel to the absolute motion of the North American plate; this is typically interpreted as the track of the Yellowstone hot spot, although alternative explanations have been proposed (e.g., Fouch, 2012). Beneath the western SRP in southwestern Idaho, fast directions trend generally E-W and delay times are high (Walker et al., 2004), with splitting patterns similar

to the HLP just to the west. Beneath the eastern SRP, fast directions are generally NE-SW, parallel to APM and to the spatiotemporal trend in the rhyolitic volcanism. This behavior persists on either side of the SRP track, as evidenced by splitting measured at a dense array (Schutt et al., 1998), and at stations located to the northwest and southeast of Yellowstone itself (Waite et al., 2005). These geographic trends are also visible in the Liu et al. (2014) dataset (Fig. 5).

Beneath the southern portion of the Cascadia subduction zone, in the region near the Mendocino Triple Junction, the deployment of onshore temporary arrays has allowed for the detailed characterization of SKS splitting patterns near the slab edge. Specifically, Eakin et al. (2010) documented a sharp rotation in ϕ at stations in northern California, with stations to the north of the triple junction exhibiting convergence-parallel fast directions and stations just to the south exhibiting NW-SE fast directions, suggesting flow around the slab edge (Fig. 6). Similarly, SKS splitting has been studied at the northern edge of the Cascadia slab by Mosher et al. (2014) using data from southwestern British Columbia. These workers found evidence for generally N-S fast directions for stations located above the Explorer microplate, which contrast with the more NE-SW fast directions above the Juan de Fuca plate. Mosher et al. (2014) interpreted these measurements as reflecting passive reorganization of the mantle flow at the slab edge, reflecting the transition from subduction-driven mantle flow in the south to mantle deformation controlled by transform motion to the north.

Beneath the Great Basin of Nevada, the unusual pattern of SKS splitting (arcuate pattern in Fig. 5) has been investigated in detail by several workers, including Savage and Sheehan (2000) and West et al. (2009). Specifically, Savage and Sheehan (2000) argued that

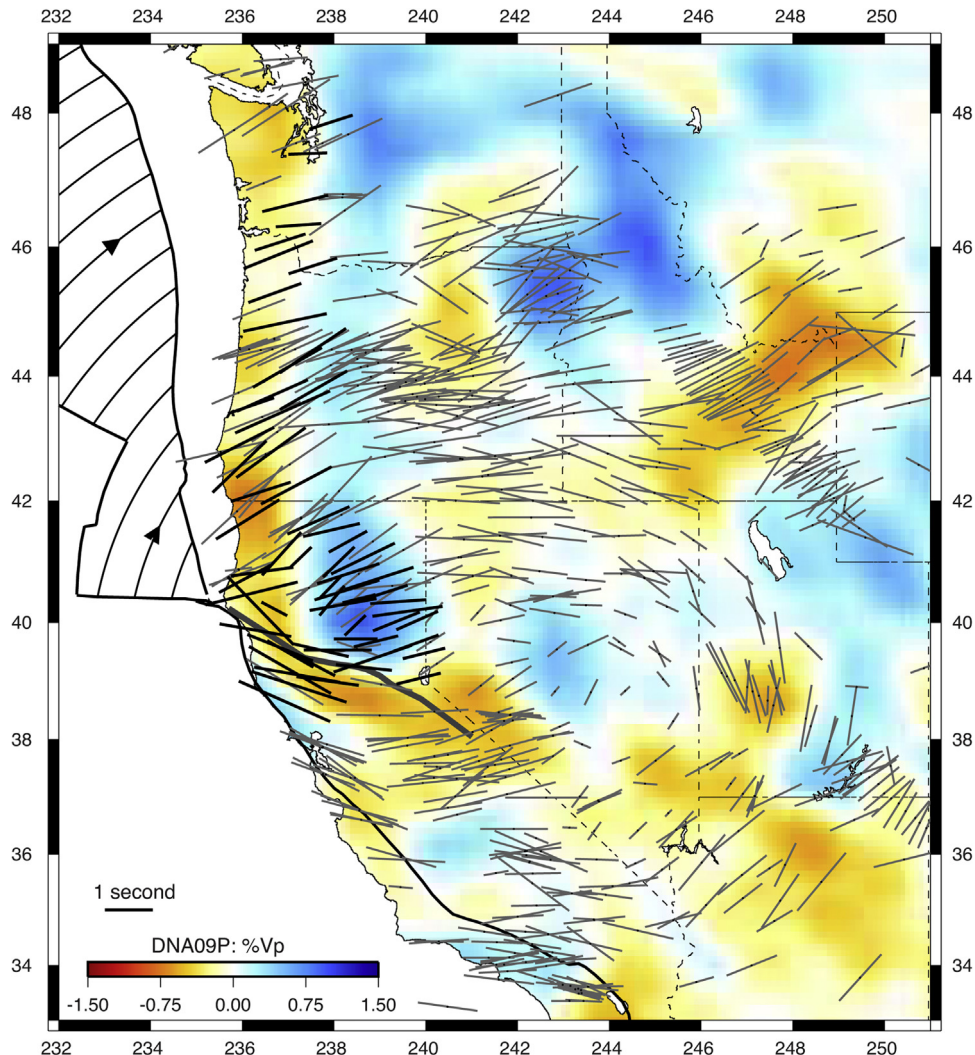


Fig. 6. Regional SKS splitting pattern overlaid on a vertically averaged upper mantle velocity anomaly (colors). The splitting results of Eakin et al. (2010) for the region around the Mendocino triple junction and the Cascadia forearc are shown with black lines; those of previous studies are shown with gray lines. The velocity anomaly shown is a vertical average over the depth range from 100 to 400 km from the P wave model of Obrebski et al. (2010). Curved black lines on the Juan de Fuca – Gorda plate indicate its absolute plate motion in a hotspot reference frame. Figure is reproduced from Eakin et al. (2010).

the generally arcuate pattern in ϕ , with smaller δt in the central portion, might be consistent with a plume-like upwelling. In contrast, West et al. (2009) combined SKS splitting analysis with tomography and numerical modeling to suggest the presence of a lithospheric “drip” (that is, a Rayleigh-Taylor downgoing instability of dense lithosphere) beneath the Great Basin. The arcuate pattern has also been invoked as evidence for large-scale toroidal flow around the edge of the slab (Zandt and Humphreys, 2008).

While most studies of shear wave splitting in Cascadia have relied on SKS phases, there is one published study of sub-slab splitting using direct teleseismic S phases originating from earthquakes within the slab and measured at distant stations. This measurement technique, known as source-side shear wave splitting (Russo and Silver, 1994), has been extensively applied in subduction zones worldwide (e.g., Lynner and Long, 2014), but it requires seismicity in the downgoing slab and is thus challenging to apply in Cascadia, which has a notable paucity of slab seismicity. Russo (2009) presented source-side splitting observations for Cascadia, although this study relied on just two events, constraining sub-slab anisotropy beneath Washington. Source-side splitting measurements beneath this region reveal evidence for strong sub-slab anisotropy, with splitting delay times typically ~ 3 s, and scattered

fast directions that may be consistent with two layers of sub-slab anisotropy. Russo (2009) argued for the presence of a layer with dominantly trench-parallel flow directly beneath the slab, with a deeper asthenospheric layer with fast directions generally parallel to the absolute motion of the Juan de Fuca plate.

2.3. Shear wave splitting results: offshore

The recent deployment of ocean bottom seismometers (OBS) on the Juan de Fuca and Gorda plates through the Cascadia Initiative (Toomey et al., 2014) has provided a unique opportunity to study the seismic anisotropy of the sublithospheric upper mantle from the ridge to the trench. Two recent papers (Bodmer et al., 2015; Martin-Short et al., 2015) have presented SKS splitting measurements for broadband OBS stations of the Cascadia Initiative (Fig. 7). For stations located on the Juan de Fuca plate, Bodmer et al. (2015) identified fast SKS directions that are nearly parallel to APM, with a small but persistent clockwise rotation. Fast directions for stations located on the Gorda plate and near the plate boundaries exhibit more heterogeneity, suggesting a diffuse shear zone that accommodates differential motion between the Gorda, Juan de Fuca, and Pacific plates. Notably, Bodmer et al. (2015) emphasize

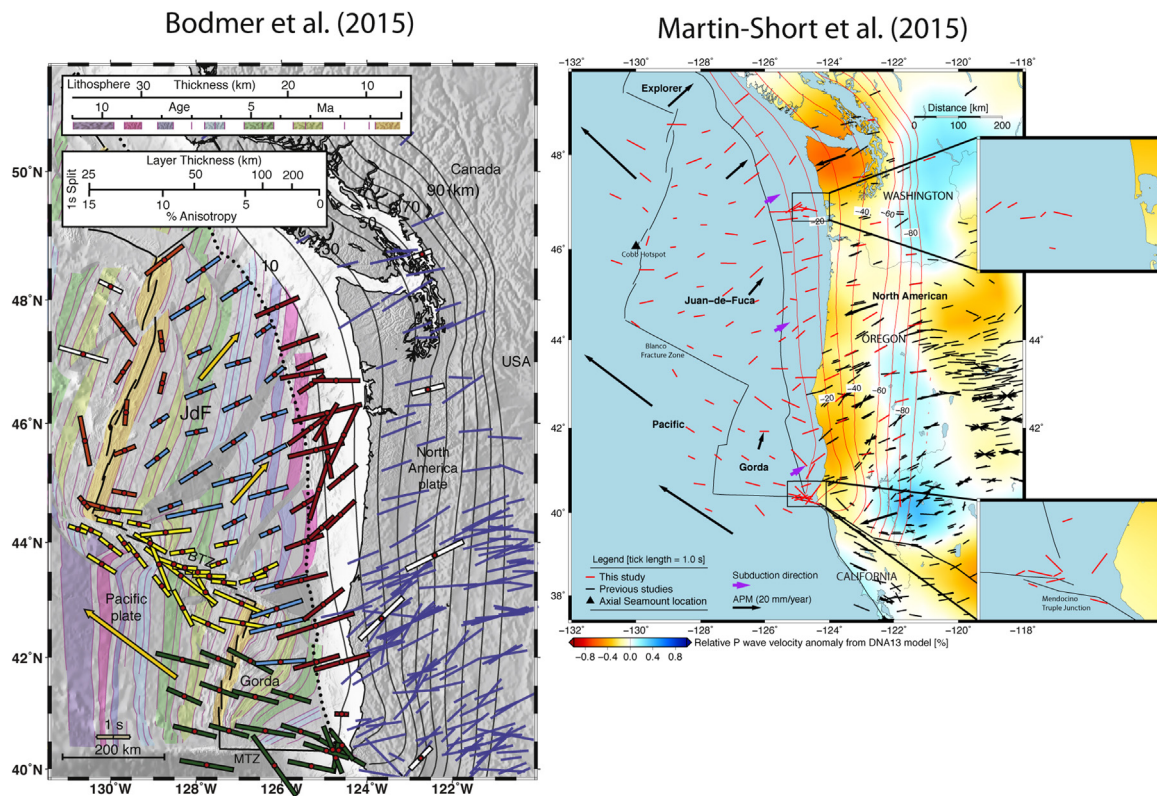


Fig. 7. Shear wave splitting measured at the offshore OBS stations deployed as part of the Cascadia initiative, reproduced from Bodmer et al. (2015, left panel) and Martin-Short et al. (2015, right panel). Left panel: stacked SKS splitting measured by Bodmer et al. (2015), plotted as colored bars at the station locations, overlaid on magnetic anomalies. Bars are color coded by zone, as explained in Bodmer et al. (2015). Yellow arrows indicate absolute plate motions; thin blue bars on land indicate previously published SKS measurements from other workers (see Fig. 4). Thin black lines indicate slab contours at 10 km intervals from McCrory et al. (2012). Right panel: stacked SKS splitting measured by Martin-Short et al. (2015), plotted as red bars at the station location that are scaled by the delay time. Black bars on land indicate previously published splitting measurements. Colors indicate tomographic P wave velocities averaged between 100 and 400 km, from Obrebski et al. (2010). Red lines indicate slab contours at 10 km intervals from McCrory et al. (2012); black arrows show the direction and magnitude of absolute plate motion in a hotspot reference frame. Purple arrows show the subduction direction, and inset maps show regions featuring a geographic concentration of splitting results.

that their dataset is inconsistent with the rollback-induced toroidal flow model; there is no evidence from the fast directions measured on the Juan de Fuca plate for a component of along-strike flow, as would be expected for the toroidal flow model. While Bodmer et al. (2015) do not rule out a component of localized flow around the slab edge in the vicinity of the Mendocino Triple Junction, as suggested by Eakin et al. (2010), they propose that it has only a secondary effect on the anisotropic structure.

Martin-Short et al. (2015) obtained fast direction patterns at Cascadia Initiative stations that are generally similar to those of Bodmer et al. (2015), increasing the confidence that SKS splitting parameters can indeed be reliably constrained even for relatively noisy OBS data. They also found evidence for ϕ that are generally parallel to APM at stations on the Juan de Fuca plate, particularly for stations located closer to the trench. This is interpreted as evidence for entrained flow beneath the downgoing slab. Martin-Short et al. (2015) implemented a series of geodynamic models to demonstrate that flow in the asthenospheric upper mantle beneath the Gorda plate is dominated by Pacific plate motion, suggesting that the small and slow-moving Gorda plate does not directly influence the flow geometry. As with the Bodmer et al. (2015) study, Martin-Short et al. (2015) do not identify evidence for the kind of large-scale toroidal flow suggested by Zandt and Humphreys (2008), which would predict a component of along-strike flow beneath the oceanic Juan de Fuca plate. However, they do suggest that their measurements in the vicinity of the Mendocino Triple Junction could be reconciled with smaller-scale flow around the slab edge, as suggested by Eakin et al. (2010), if the toroidal compo-

nent of flow driven by slab rollback is accommodated in the deeper mantle (depths greater than ~400 km).

2.4. Other observations: surface waves, receiver functions, and anisotropy tomography

In addition to shear wave splitting, other seismic observations such as anisotropic surface and body wave tomography, transverse component receiver function analysis, and Love-to-Rayleigh wave scattering also constrain anisotropic structure, especially its variation with depth. Surface wave tomography that includes anisotropic parameters, in addition to isotropic wavespeed variations, has been applied to data from the TA and other deployments in the PNW. This includes studies that have considered anisotropic phase velocity maps at different periods, as well as those that directly invert for anisotropy as a function of depth, and encompasses studies that have examined ambient noise, event-based surface waves, or a combination of the two. For example, Beghein et al. (2010) examined anisotropic phase velocity maps for the region beneath the Great Basin of Nevada, and found evidence for an arcuate pattern of azimuthal anisotropy at lithospheric depths, with evidence for varying patterns of fast directions in the asthenospheric upper mantle. They argued that the anisotropy patterns revealed by surface waves in the asthenosphere were not obviously compatible with the Zandt and Humphreys (2008) toroidal flow model, but could be reconciled with the lithospheric drip model of West et al. (2009).

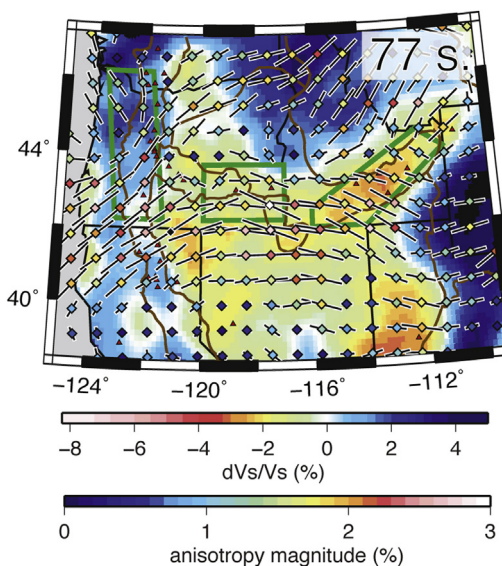


Fig. 8. Results of anisotropic Rayleigh wave phase velocity inversion at a period of 77 s, from the model of Wagner and Long (2013). Peak sensitivity at this period is in the uppermost mantle, at depths of approximately 75 km. Background colors show deviations in shear velocity from the starting model, as shown by the top color bar. Fast directions of anisotropy are shown by the black bars. Strength of anisotropy is denoted by both the color of the diamond at each node (bottom color bar) and by the length of the bars. Green boxes indicate regions with particularly striking anisotropy, including eastern Oregon, the Snake River Plain, and the Cascades arc region, which at shorter periods (not shown) exhibits strong trench-parallel anisotropy. At 77 s period (shown), strong E-W anisotropy beneath eastern Oregon is visible, along with a hint of an arcuate pattern in fast directions surrounding the Great Basin, similar to that found in SKS splitting patterns (Fig. 4). Source: Figure reproduced from Wagner and Long (2013).

A more regionally extensive model for the western US that combines constraints from surface waves and SKS splitting (Yuan and Romanowicz, 2010) displays azimuthal anisotropy that varies with depth and is able to reproduce the arcuate pattern in SKS fast splitting directions, with smaller delay times in the central Basin and Range. Yuan and Romanowicz (2010) interpret this pattern as reflecting a combination of plate-driven shearing and interactions between mantle flow and the craton edge. It is notable that the Yuan and Romanowicz (2010) model also features particularly strong anisotropy beneath the High Lava Plains region that is coherent with depth, consistent with the large shear wave splitting delay times observed there (Long et al., 2009). Another model with similar geographic coverage that combines constraints from ambient noise as well as event-based surface waves is that of Lin et al. (2011), who constrained anisotropy in the mid-to-lower crust, the uppermost mantle (which probably mostly reflects the lithosphere), and asthenosphere beneath the western US. Lin et al. (2011) find evidence for asthenospheric fast directions that are parallel to Juan de Fuca–North America convergence to the north of the Mendocino Triple Junction. They also find a general pattern of E-W fast directions elsewhere that they interpret as resulting from a combination of plate motions and slab-driven flow. Evidence for toroidal flow from this model is mixed, although there is a distinct transition from NE-SW fast directions near the Cascadia arc to more E-W fast directions in the backarc.

Another anisotropic surface wave model with a tighter focus on the PNW has also been presented in Wagner et al. (2013) and Wagner and Long (2013). Anisotropic phase velocity maps for this model (Fig. 8) at longer periods (~77 s and greater) show some evidence for an arcuate pattern in fast directions (Wagner and Long, 2013), similar to what is predicted for the Zandt and Humphreys (2008) toroidal flow model. As with the Lin et al. (2011) model, there is evidence for a distinct transition from fast directions that

are parallel to the convergence direction in the arc and forearc region to fast directions that are generally E-W (beneath the High Lava Plains of Oregon) or dominated by an arcuate pattern (beneath northern Nevada). Interestingly, this model also yields evidence for a localized region of trench-parallel fast directions in the Cascadia forearc, which was interpreted as being due to CPO of serpentinite phases (Wagner et al., 2013).

Constraints on *P* wave anisotropy beneath the Pacific Northwest come from body wave tomographic models that include anisotropy as a parameter, using either teleseismic and regional *P* waves (Huang and Zhao, 2013) or *Pn* phases from regional earthquakes that sample the uppermost mantle (Buehler and Shearer, 2010). At a depth of 50 km, the *P* wave anisotropy model of Huang and Zhao (2013) shows some evidence for an arcuate pattern in fast directions around the Great Basin, but other features do not match well with inferences from other types of data. For example, beneath the Cascadia arc and forearc region the model at 50 km depth exhibits fast directions that are nearly orthogonal to the convergence direction. At a depth of 100 km, the Huang and Zhao (2013) model exhibits complex patterns of fast directions that generally contrast with SKS splitting patterns beneath the PNW (their Fig. 9). The *Pn* anisotropy model of Buehler and Shearer (2010) for the most part likely reflects anisotropy in the lithospheric uppermost mantle, and does not directly reflect present-day mantle flow. Nevertheless, a comparison between *Pn* anisotropy SKS splitting (Fig. 9 of Buehler and Shearer, 2010) argues for a significant contribution from the asthenospheric upper mantle to SKS splitting parameters, as the geometry of anisotropy in the uppermost (lithospheric) mantle inferred from *Pn* does not generally provide a complete explanation for SKS observations.

Receiver functions can also place constraints on anisotropic structure at depth, specifically through the analysis of azimuthal variations in radial and transverse component energy. This technique has been applied to data from the Cascadia subduction zone by several workers (Park et al., 2004; Nikulin et al., 2009), and is particularly effective at delineating sharp contrasts in anisotropy at interfaces such as the top of the subducting slab. Park et al. (2004) and Nikulin et al. (2009) both identified evidence for serpentized and deformed mantle just above the subducting Cascadia slab, at depths of ~40 km, using receiver function analysis. These results, however, mainly constrain the geometry of anisotropy in the layer of mantle wedge directly above the slab, and are less relevant to considerations of the large-scale mantle flow field.

Finally, observations of quasi-Love wave propagation have been used to constrain the large-scale geometry of seismic anisotropy in the Cascadia subduction system (Rieger and Park, 2010). Quasi-Love waves result from the scattering of Love wave energy to Rayleigh wave energy in the presence of a sharp gradient in anisotropy (e.g., Levin et al., 2007b). Rieger and Park (2010) documented observations of quasi-Love waves arriving at EarthScope stations in the PNW, originating from earthquakes in the western Pacific, and inferred to reflect anisotropy in the asthenospheric upper mantle in the offshore portion of the Cascadia subduction zone. They further documented azimuthal variations in the amplitude of the quasi-Love phases that were consistent with an anisotropic fast direction parallel to Juan de Fuca plate motion and the subduction convergence direction. From this, Rieger and Park (2010) argued for the presence of two-dimensional entrained flow beneath the Juan de Fuca slab in the upper mantle.

3. Observations of volcanism and geochemistry

Seismologists often point to seismic anisotropy as the most direct observable that constrains patterns of mantle flow; however, equally powerful observational constraints on flow patterns come

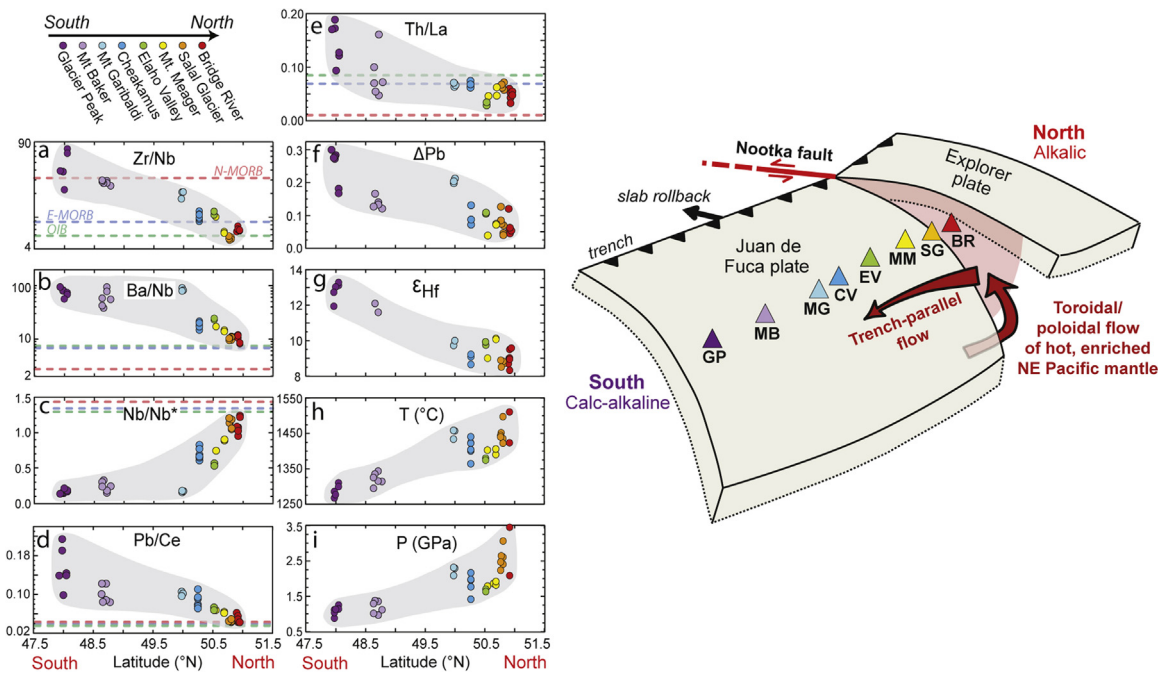


Fig. 9. Geochemical data from the Garibaldi Volcanic Belt at the northern edge of the Cascadia subduction zone and interpretation in terms of mantle flow, from Mullen and Weis (2015). Left: Geochemical data are plotted as a function of latitude (south to north) for a variety of geochemical tracers, as indicated by each figure label, along with temperature (panel h) and pressure (panel i) calculated from a silica activity geobarometer and olivine-liquid geothermometer. Details of tracers and calculations can be found in Mullen and Weis (2015). Right: Schematic 3D representation of plate configuration at the northern end of the Cascade Arc, along with inferred mantle flow (red arrows). In this model, there is an influx of hot, enriched NE Pacific mantle through the slab gap by toroidal/poloidal flow, triggered by slab rollback (heavy black arrow). Southerly narrowing of the second arrow depicts the waning influence of NE Pacific mantle on magma compositions due to progressive mixing with melts of the depleted mantle wedge. Source: Figure is reproduced from Mullen and Weis (2015).

from geochemical tracers. Specifically, if geochemical signatures that are particular to a certain mantle reservoir can be identified, then their evolution in space and time (as expressed in volcanic rocks) can be used to map patterns of mantle flow. For example, Turner and Hawkesworth (1998) argued that a combination of geochemical tracers (including helium and lead isotope ratios along with incompatible element ratios) can be used to map mantle flow beneath the Lau Basin in the northern part of the Tonga subduction system. They argued for the infiltration of Samoan plume material (based on its distinctive $^3\text{He}/^4\text{He}$ ratio) in a trench-parallel direction into the mantle wedge, arguing for an along-strike component of mantle flow. Similarly, Hoernle et al. (2008) combined evidence from Pb and Nd isotope ratios and their variation along the Central American volcanic arc with evidence from seismic anisotropy in the mantle wedge to argue for along-strike flow above the subducting Cocos plate, at a rate roughly comparable to the downgoing plate velocity.

Recently, Mullen and Weis (2015) applied geochemical analysis to basalts from the northern part of the Cascades (the Garibaldi Volcanic Belt, Fig. 1) and argued for a component of trench-parallel flow in the mantle wedge based on along-strike variability in trace element and isotope ratios. Specifically, they examined a suite of trace elements and isotope ratios for Sr, Nd, Hf, and Pb and documented spatial variations from north to south (that is, near the slab edge to near the slab interior) along the volcanic belt for most of the geochemical indicators studied (Fig. 9). They propose that these trends reflect a greater extent of mantle depletion and a higher proportion of melt contributions derived from the slab with increasing distance from the slab edge. Mullen and Weis (2015) suggest that the geochemical observations are consistent with toroidal mantle flow driven by slab rollback at the northern edge of the Cascadia slab, and point to the consistency among the observed geochemical gradients, seismic anisotropy indications, and predictions from

geodynamic models (discussed in section 4 below) as further support for the toroidal flow model.

In addition to observations from basalt geochemistry, the spatiotemporal patterns and petrologic characteristics of volcanics can themselves shed light on the processes in the underlying mantle that cause melting. Studies of volcanism in the Oregon backarc have played a key role in the formulation of hypotheses that address present-day mantle dynamics. The pattern, timing, and characteristics of backarc volcanism in eastern Oregon, which is dominated by the bimodal and partially time-progressive High Lava Plains (HLP) volcanic province, have proven to be challenging to explain in the context of mantle dynamics models for the Pacific Northwest (e.g., Carlson and Hart, 1987; Camp and Hanan, 2008; Faccenna et al., 2010; Foulger et al., 2015). This is perhaps particularly true for those models that invoke a deep mantle plume as the source of both the Columbia River flood basalts and later volcanism in the HLP and the Yellowstone/Snake River Plain (Y/SRP) to its east (e.g., Camp and Ross, 2004; Jordan, 2005; Smith et al., 2009; Camp, 2013).

The High Lava Plains region of eastern Oregon includes both time-progressive rhyolitic volcanism that has migrated to the west-northwest over the past 12 Ma, as well as basaltic volcanism that is widespread in space and time. A recent investigation of the spatiotemporal trends of HLP volcanism (Ford et al., 2013) contradicts the predictions of a model that invokes motion of the North American plate over a stationary mantle upwelling, similar to the conclusions of previous workers (e.g., Jordan, 2005). New $^{40}\text{Ar}/^{39}\text{Ar}$ dates presented by Ford et al. (2013) show clear evidence for a westward migration of rhyolitic volcanism at a rate of roughly 33 km/Ma, with a slowing of this rate around 4 Ma. Ford et al. (2013) relate this rhyolitic trend to mantle flow processes that result from the rollback and steepening of the Cascadia slab, and argue that the mantle flow geometry inferred from the age progression of the rhyolites is identical to the flow direction inferred from SKS splitting beneath the HLP, as documented by Long et al. (2009).

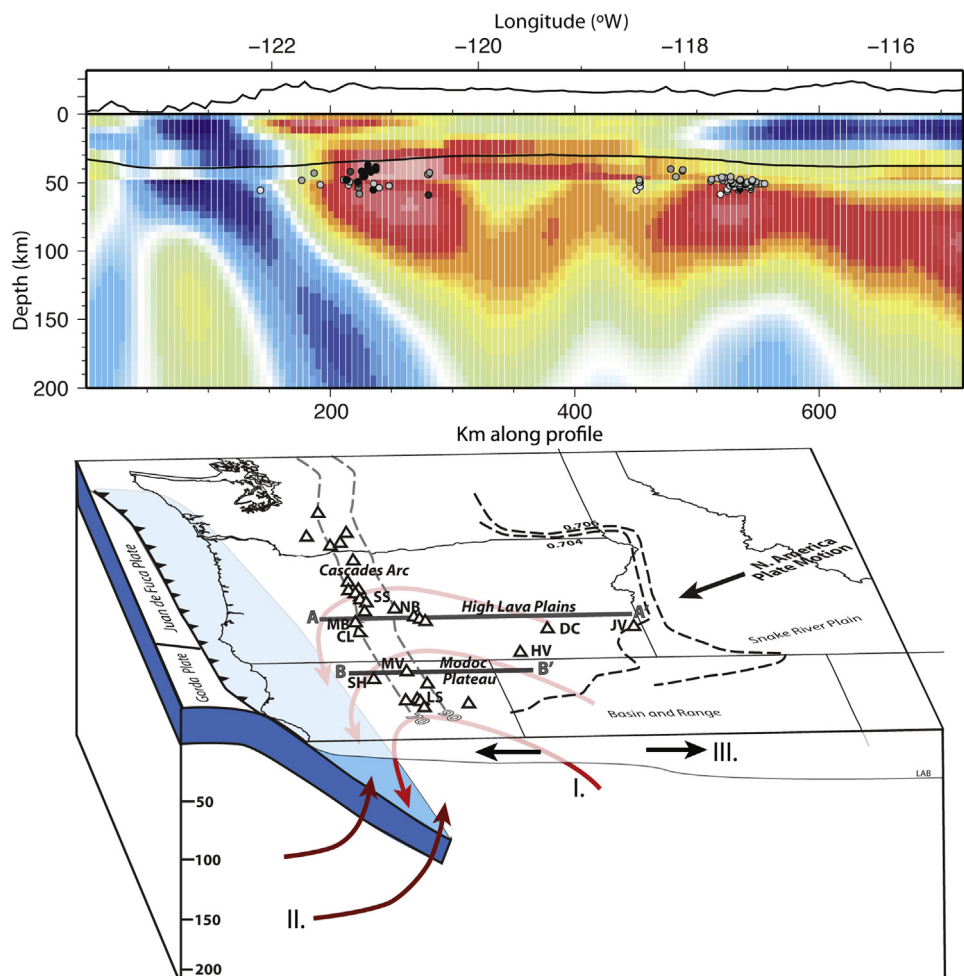


Fig. 10. Results and interpretation of basalt thermobarometry from the work of Till et al. (2013). Top panel: NW-SE cross-section of depths and temperatures of origin for Holocene basalts (circles) from the High Lava Plains and central Oregon Cascades, plotted on top of the shear wave tomography model of Wagner et al. (2010) at mantle depths and Hanson-Hedcock et al. (2012) for the crust; magnitudes of relative shear velocity variations are shown in color, varying from 5% fast (blue) to 9% slow (white). Figure from Long et al. (2012). Grayscale of the circles indicates the basalt temperatures, ranging from 1220 °C (black) to 1390 °C (white). Bottom panel: Cartoon interpretation illustrating three potential causes of mantle upwelling that likely produced the primitive basalts with low pre-eruptive H₂O contents in southern Oregon and northern California: (I) subduction-induced corner flow in the mantle wedge, (II) toroidal flow around the southern termination of the subducting slab, and (III) northwest Basin and Range crustal extension. Gray-dashed lines represent depth contours for the subducting slab, while black-dashed lines indicate the approximate location of the $^{87}\text{Sr}/^{86}\text{Sr}$ 0.704 and 0.706 lines that coincide with the western margin of Precambrian North America (see Till et al., 2013 for details). Source: Figure reproduced from Till et al. (2013)gr10

The physical conditions associated with the mantle melting that produced young volcanism beneath the HLP was investigated by Till et al. (2013), who applied thermometry and barometry techniques to a suite of primitive, anhydrous basalts from the HLP and surrounding regions. Till et al. (2013) found evidence for melt extraction at roughly 40–58 km depth beneath the HLP, just beneath the geophysically imaged Moho (e.g., Eagar et al., 2011), at temperatures (between 1185 and 1383 °C) that are relatively warm, but not hot enough to require a contribution from a deep mantle plume. Till et al. (2013) further argue that the conditions of melting inferred from their study are consistent with upwelling associated with a combination of subduction-driven corner flow and toroidal flow around the southern edge of the slab (Fig. 10). This proposed style of decompression melting and volcanism associated with toroidal flow around a slab edge is similar to scenarios that have been suggested for other regions, notably volcanism at Mt. Etna associated with the edge of the Ionian slab (Schellart, 2010).

4. Geodynamic modeling constraints

Insights gained from geodynamic modeling are critical for an understanding not only of mantle flow patterns, but of the phys-

ical processes that drive mantle flow (e.g., Billen, 2008; Gerya, 2011; Jadamec, 2016; Schellart and Strak, 2016). A series of analog modeling experiments was carried out in order to investigate specific aspects of Cascades backarc volcanism, particularly the roles of subduction-driven flow and/or a possible mantle plume in producing HLP volcanism and other volcanic features (Druken et al., 2011; Kincaid et al., 2013). These laboratory experiments used a kinematic-dynamic subduction model to understand the patterns of flow in the Cascadia subduction system and to predict observables such as seismic anisotropy and spatiotemporal trends in volcanism. Specifically, Druken et al. (2011) carried out a series of experiments with parameters appropriate for modeling Cascadia subduction, including a phase of trench rollback beginning at ~20 Ma. They found that a combination of slab rollback and a modest amount of upper plate extension produced a large-scale toroidal flow field that produced efficient alignment of strain markers in an E-W direction in the portion of the model corresponding to the HLP, providing an excellent match to the SKS splitting observations of Long et al. (2009). The suite of models presented by Druken et al. (2011) was further explored in the synthesis of Long et al. (2012) to understand the implications of large-scale toroidal flow for patterns of volcanism and the thermal evolution of the system.

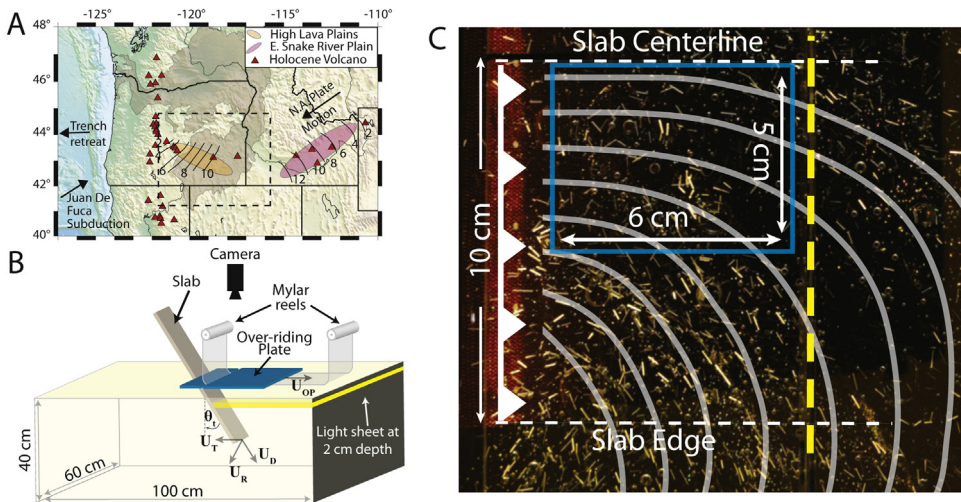


Fig. 11. Model setup and results for the laboratory models of mantle flow described in Druken et al. (2011). (a) Tectonic setting of the Pacific Northwest, indicating the basic kinematic elements that the model aims to reproduce. Brown shaded region indicates the extent of the S/CRB flood basalts; red triangles indicate Holocene volcanics. Thin black lines indicate approximate age contours of rhyolitic volcanism within the HLP and SRP trends. Black arrows indicate the absolute plate motion direction of the North American plate, the convergence direction of the Juan de Fuca plate relative to North America, and the absolute migration of the trench, respectively. Dashed box indicate the region under study. (b) Cartoon sketch of the kinematic subduction model, which includes a tank of glucose syrup that simulates mantle flow, Mylar reels that simulate the motion of the downgoing and overriding plates, and a trench that migrates with respect to the tank. (c) Map-view image of illuminated model slice from a typical experiment, showing whiskers (small white lines) that locally align with finite strain in the fluid and generally match the observations of fast splitting directions from Long et al. (2009). The yellow dashed line and blue box indicate the overriding plate extension center and area of interest for this study, respectively. Approximate instantaneous streamlines for the flow field are shown in gray, indicating the presence of large-scale toroidal flow. Source: Figure reproduced from Druken et al. (2011).

Long et al. (2012) highlighted the prediction of a distinctive pulse of upwelling approximately ~3 Myr after the initiation of rollback and steepening, along with continuing migration of a front of elevated temperatures at the base of the overriding plate to the west at a rate that is consistent with the observed temporal progression of rhyolitic volcanism in the HLP (Ford et al., 2013) (Fig. 11). An important conclusion from the modeling work of Druken et al. (2011), then, is that relatively simple plate forcing (downdip motion, rollback, and steepening of the slab) can result in complex, three-dimensional, time-varying flow fields. Furthermore, models that are dominated by large-scale toroidal flow are capable of reproducing the pattern of anisotropy observed in the Oregon backarc as well as first-order characteristics of backarc volcanism, including the timing and location of the S/CRB flood basalts and subsequent volcanism in the HLP (Druken et al., 2011; Long et al., 2012).

A second modeling study (Kincaid et al., 2013) used a similar set of kinematic boundary conditions as the Druken et al. (2011) study, but also included a thermal plume at the bottom of the model volume and investigated the interaction of the plume with subduction-driven mantle flow. This study found that a buoyant plume may be bifurcated within the complex flow field induced by subduction, potentially explaining first-order aspects of PNW geologic and volcanic history. Specifically, the western portion of the plume anomaly in the models of Kincaid et al. (2013) can become entrained into the slab-driven flow field, potentially explaining the age progression in HLP rhyolites, while the eastern portion migrates in a geometry consistent with the SRP age progression. Importantly, a major conclusion from the work of Kincaid et al. (2013) is that plume material, if present, effectively acts as a passive tracer within the subduction-induced flow field; while the presence of the hot plume can explain patterns of volcanism, it does not substantially modify the flow field itself.

Other workers have investigated the possible relationships between the behavior of the Juan de Fuca slab in the upper mantle and surface volcanism from a geodynamic modeling perspective (e.g., Schellart et al., 2010; Liu and Stegman, 2012). For example, Liu and Stegman (2012) implemented a suite of numerical models that incorporated data assimilation and found that the model that

provides the best fit to present-day tomographic models of mantle structure includes an episode of slab tearing that is consistent in both space and time with the S/CRB flood basalt eruptions. These models feature complex and time-varying flow fields that would likely predict complicated patterns of present-day upper mantle anisotropy in the backarc, although detailed comparisons between predicted and observed anisotropy have not yet been carried out. Later work carried out using a similar modeling approach by Leonard and Liu (2016) investigated possible interactions between the sinking Juan de Fuca slab and a possible deep-seated mantle plume; based on this series of models, the authors argued that the presence of a deep mantle plume to the formation of Yellowstone volcanism may be less important than previously thought. Importantly for the arguments made in the present paper, Leonard and Liu (2016) found that the evolution of mantle structures and the character of the mantle flow field are dominated by the sinking slab, similar to the findings of Kincaid et al. (2013) for their plume-slab interaction models. Taken together, these studies suggest that subduction-controlled processes are the most important in controlling the mantle flow field, and that present-day mantle flow in the Cascadia subduction system is likely complex and three-dimensional, regardless of the presence or absence of a mantle plume.

In addition to these modeling studies that are specific to the Cascadia subduction system, a number of papers address the presence and characteristics of three-dimensional flow in subduction systems from a modeling perspective. Modeling studies that use both numerical (Faccenda and Capitanio, 2013; Li et al., 2014) and analog (Piromallo et al., 2006; MacDougall et al., 2014; Strak and Schellart, 2014, 2016; Chen et al., 2016) approaches have investigated toroidal flow in subduction systems, often with the explicit goal of comparing with seismic anisotropy observations. Particularly relevant to the discussion here, Faccenda and Capitanio (2013) modeled the flow field and resulting anisotropy for a fully dynamic slab with trench rollback, and predicted a complex flow field that featured mostly trench-normal fast splitting directions in the backarc, consistent with what is observed in the Cascadia subduction zone. Similar models by Li et al. (2014) also documented

this geometry of anisotropy in the central portion of the model backarc in subduction models with significant rollback. This type of behavior – with toroidal flow due to slab rollback focusing strong trench-normal flow in the central portion of the backarc, with more complex flow fields near the edges of the slab – also manifests in analog experiments, such as those of MacDougall et al. (2014) for a series of model geometries that included slab gaps and variable slab dips.

A series of analog models by Schellart and collaborators (Schellart et al., 2010; Strak and Schellart, 2014, 2016; Chen et al., 2016) has investigated the role of slab width and trench rollback in the behavior of slabs, including both their kinematics and the character of mantle flow induced by subduction. For example, Strak and Schellart (2014) demonstrated that upwelling associated with toroidal flow around slab edges is a common feature, providing support for the hypothesized link between toroidal edge flow and volcanism near slab edges (e.g., Schellart, 2010; Till et al., 2013). Later work explicitly investigated how the character of this upwelling is affected by the width of the slab (Strak and Schellart, 2016) and how the flow induced by rollback subduction interacts with the overriding plate, perhaps resulting in backarc extension (Chen et al., 2016).

5. Possible fragmentation of the Juan de Fuca slab at depth

Many of the geodynamic models of mantle flow discussed in Section 4 include an intact subducting slab – either one that is planar and kinematically defined (e.g., Piromallo et al., 2006; Druken et al., 2011; Kincaid et al., 2013) or one that is deformable and dynamic (e.g., Faccenda and Capitanio, 2013; Li et al., 2014). Models that feature large-scale toroidal flow around the edges of a subducting slab due to slab rollback, with focusing of trench-normal return flow in the central portion of the backarc, generally feature an intact slab that serves as an efficient barrier to lateral flow as the slab rolls back, forcing material around the slab edges (e.g., Paczkowski et al., 2014). In contrast, models in which the slab breaks up, or has gaps, tend to feature focused flow through the slab gaps instead of a well-organized toroidal flow field (e.g., Liu and Stegman, 2012; MacDougall et al., 2014). Therefore, the viability of large-scale toroidal flow as an explanation for shear wave splitting patterns in the Pacific Northwest, as suggested by Zandt and Humphreys (2008) and later workers (e.g., Fouch and West, 2008; Long et al., 2012), hinges on the ability of the Juan de Fuca slab to act as a barrier to flow in the upper mantle. Recent work to image the Juan de Fuca slab at depth, relying on data from USArray and related efforts, has suggested instead that the slab may be fragmented both in the mid-mantle (transition zone depths and deeper) and in the upper mantle. The question of whether the upper mantle portion of the slab is fragmented, and thus whether it can induce a large-scale toroidal flow field, is critically important for understanding mantle flow beneath Cascadia.

One of the most important scientific results to come out of the tomographic imaging efforts using USArray seismic data is the finding that mantle seismic structure beneath the PNW is highly complex and suggests a complicated slab morphology (e.g., Becker, 2012; Pavlis et al., 2012). At mid-mantle depths, a number of studies have argued for the fragmentation of the slab and for a complex relationship between past subduction history and present-day mantle structure (e.g., Obrebski et al., 2011; Sigloch, 2011; James et al., 2011). To highlight one example, James et al. (2011) argued that a relatively fast anomaly in tomographic models at depths between 400 and 600 km roughly beneath the Y/SRP hotspot track corresponds to an “orphaned” piece of Farallon slab in the mid-mantle, providing evidence for slab fragmentation in the mid-mantle that generally agrees with findings from other authors

(e.g., Obrebski et al., 2011; Sigloch, 2011). However, a fragmented slab at mid-mantle depths can likely be reconciled with the toroidal flow model if the slab is intact in the upper mantle, as long as there is a viscosity jump in or near the transition zone that acts as a partial barrier to return flow beneath the subducting slab, as shown in the modeling experiments of Paczkowski et al. (2014). A critical question, therefore, is to what degree the slab is fragmented at depths above ~400 km in the upper mantle.

While the Juan de Fuca slab is clearly imaged as a relatively fast anomaly in the upper mantle in most tomography models, its continuity and depth extent are debated. Some workers image the slab down to a depth of ~300 km in body wave models but argue that the slab anomaly does not extend to the deepest portion of the upper mantle (e.g., Obrebski et al., 2010; Darold and Humphreys, 2013); however, other authors have argued for a continuous slab anomaly that reaches into the transition zone (e.g., Roth et al., 2008), particularly in the southern portion of the subduction system. A robust feature of many upper mantle tomography models is the along-strike variability in the strength of the slab velocity anomaly at depths around 100–150 km, and the possible presence of a “gap” in the slab at upper mantle depths near the Oregon-Washington border (e.g., Roth et al., 2008; Obrebski et al., 2010; Wagner et al., 2010; Schmandt and Humphreys, 2010; Porritt et al., 2011; Darold and Humphreys, 2013; Gao and Shen, 2014) (Fig. 12).

It is debated, however, to what extent this feature in the seismic wave speed models corresponds to actual slab fragmentation in the upper mantle. For example, Obrebski et al. (2010) argued for a slab rupture and breakup at approximately ~19 Ma associated with the impingement of the Yellowstone plume head on the slab; this slab breakup, in their model, resulted in the present-day fragmentation of the slab in the upper mantle. Later work by this group (Obrebski et al., 2011) reiterated the argument for a gap in the slab beneath ~150 km depth in northern Oregon, a view shared by other authors (e.g., Schmandt and Humphreys, 2010). However, other workers have argued against this notion, positing that the apparent slab gap (as expressed in substantial weakening of the slab-related fast anomaly) near the Oregon-Washington border may be an artifact associated with imperfect resolution due to the major slow anomaly in the mantle wedge just to the east of the purported gap (Roth et al., 2008). Some models (e.g., Wagner et al., 2010; Chen et al., 2015) seem to show the fast slab anomaly to be nearly continuous along strike to depths of ~150 km or greater, although there are along-strike variations in its strength.

What are we to conclude about the contiguity of the Juan de Fuca slab in the upper mantle based on tomographic imaging? As pointed out by Roth et al. (2008) and others, the resolution of tomographic models beneath the Pacific Northwest is imperfect, despite the good data coverage afforded by USArray, and the presence of major slow anomalies in the mantle wedge may hamper the ability of the data to resolve a possible fast slab anomaly. Furthermore, although the first-order patterns in various western US tomography models tend to be similar, their amplitudes vary significantly (e.g., Becker, 2012), and a straightforward extrapolation to temperature and/or composition (or subduction history) is difficult. Furthermore, the presence of strong seismic anisotropy in the upper mantle beneath the PNW could potentially bias tomographic inversions, most of which assume isotropic structure (e.g., Bezada et al., 2016). The structures retrieved in tomographic imaging can depend strongly on the starting model; for example, Chen et al. (2015) carried out inversions with a slab-like fast structure in the starting model rather than relying on a 1-D starting model; when an *a priori* slab was included, the retrieved slab structure appears to be more continuous than in other models that fit the data equally well.

Other seismic imaging methods can provide constraints on slab structure that are complementary to those provided by tomogra-

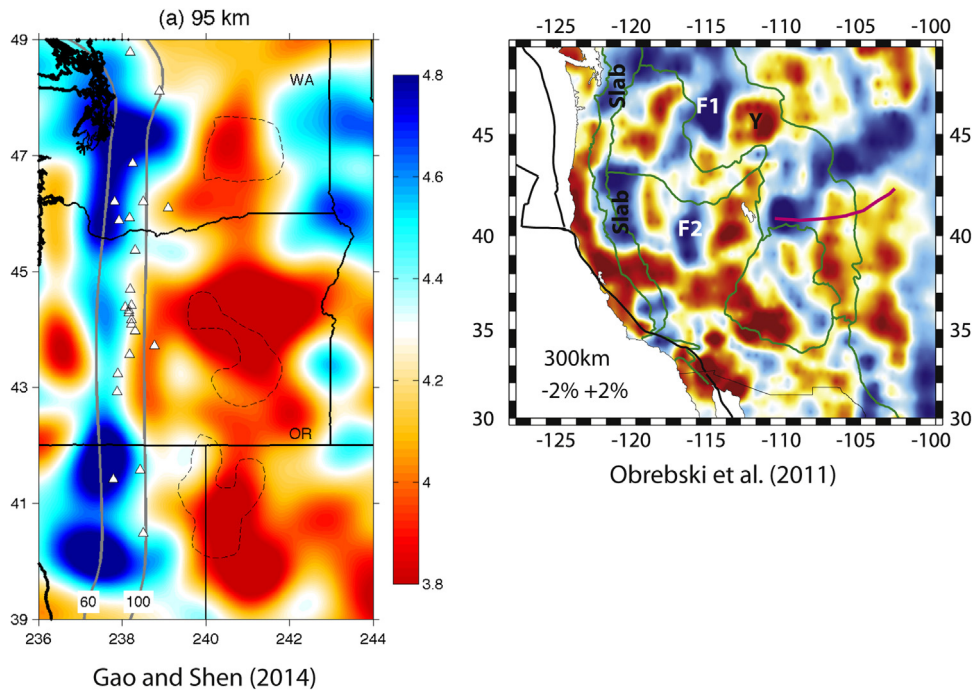


Fig. 12. Horizontal slices through two different shear wave velocity models for the PNW, demonstrating evidence for fragmentation of the slab in the upper mantle. Left panel: Horizontal slice at a depth of 94 km from the model of Gao and Shen (2014); colors correspond to shear velocity in km/sec, as indicated by the color bar. The slab corresponds to the N-S trending fast anomaly (blue), which is clearly weaker in the central part of the arc. Figure reproduced from Gao and Shen (2014). Right panel: Horizontal slice at a depth of 300 km from the S wave model of Obrebski et al. (2011). Color scale used to represent the velocity anomalies ranges from +2% deviations from the starting model (blue) to –2% deviations (red). Green lines indicate physiographic provinces; magenta line indicates the Cheyenne Belt. A number of fast anomalies are imaged at this depth; particularly relevant is the apparent gap in the slab just to the east of the Cascades arc (two inferred fragments are labeled “Slab”). Source: Figure reproduced from Obrebski et al. (2011).

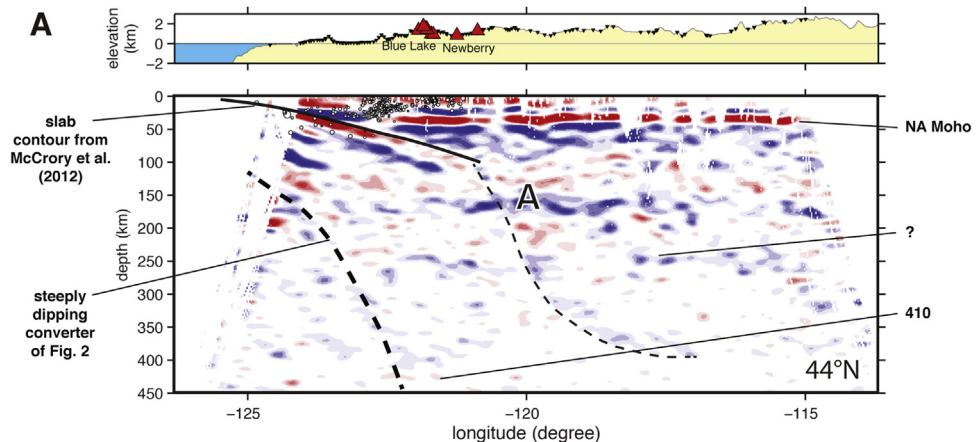


Fig. 13. Reflectivity profile of the Cascadia subduction zone at a latitude of 44.25°N along a profile across central Oregon, from Tauzin et al. (2016). Red/blue areas show positive/negative amplitudes corresponding to increases/decreases of V_s , respectively. The seismicity above and below the slab is indicated with open circles; the depth contour of the Gorda-Juan de Fuca plate from McCrory et al. (2012) is plotted with a black line. The dashed lines are inferred from reflectivity and seismic tomography (e.g., Fig. 10) and indicate the possible boundary delimiting the subducted plate from the mantle wedge. Source: Figure reproduced from Tauzin et al. (2016).

phy, and waveform modeling methods as well as scattered wave imaging methods have been applied to the Cascadia subduction zone. Chu et al. (2012) applied waveform modeling techniques to a suite of models derived from seismic tomography, and found evidence for the downdip extent of the subducted slab to a depth of ~250 km beneath Seattle and a shallower depth beneath Portland, consistent with the idea that the slab does not extend continuously to the base of the upper mantle. However, recent imaging of the slab using a multiple mode conversion technique by Tauzin et al. (2016) provides a different view of slab structure (Fig. 13). These workers obtain a reflectivity image of the upper mantle down to a depth of 450 km beneath Cascadia, and find evidence for conver-

sions associated with the slab in the depth range of the “slab gap” inferred from tomography. They conclude, therefore, that although the slab might not manifest in tomographic images of mantle wave speed, a contiguous (or nearly so) subducted plate is in fact present down to the base of the upper mantle (Tauzin et al., 2016).

6. The Cascadia Paradox: where do we stand?

The geophysical, geochemical, and other data that shed light on mantle flow in the Cascadia subduction system lend themselves to varying and often conflicting interpretations. On balance, there is compelling evidence for at least some component of toroidal

flow; observations that support this view include shear wave splitting observations at the edges of the slab (e.g., Eakin et al., 2010; Mosher et al., 2014; Martin-Short et al., 2015) and geochemical observations that suggest a component of along-strike material transport in the mantle wedge (Mullen and Weis, 2015). What is not clear, however, is whether any three-dimensional component of flow is a small-scale phenomenon localized to the area near the slab edges, or whether there is a large-scale component of toroidal flow extending well into the backarc, such as that advocated by Zandt and Humphreys (2008). Given that both of the simplest end-member models (two-dimensional entrained flow both above and beneath the slab, vs. large-scale three-dimensional toroidal flow induced by slab rollback) are commonly invoked in the literature as explanations for observations, it is clear that the Cascadia Paradox has not yet been resolved.

At the heart of this uncertainty is the fact that there are clear and convincing observations in different portions of the subduction system that seem to lead inexorably to different conclusions about mantle flow patterns. For example, there are now several lines of evidence that suggest that the suboceanic upper mantle offshore Cascadia is dominated by plate motion parallel shearing, with fast anisotropy directions that are parallel to the motion of the Juan de Fuca plate. This includes recent shear wave splitting measurements at OBS stations of the Cascadia Initiative array (Bodmer et al., 2015; Martin-Short et al., 2015), but also includes observations of Love-to-Rayleigh wave scattering due to offshore structure (Rieger and Park, 2010), which exhibit amplitude variations with azimuth that are consistent with entrained sub-slab flow. The predictions made by the simplest entrained flow models, however, are not borne out by SKS splitting observations on the overriding plate (Fig. 5); it is clear that other processes influence these anisotropy patterns, whether these processes include 3-D toroidal flow, lithospheric delamination, frozen lithospheric anisotropy from past deformation episodes, or a combination of these.

Among the most compelling observations that argue for large-scale toroidal flow in the Cascadia subduction system are observations and models of seismic anisotropy beneath the central portion of the backarc, most notably the HLP region. The initial observation of an arcuate pattern of SKS fast orientations in the western US (Zandt and Humphreys, 2008) in pre-TA compilations has generally held up in the post-TA era (e.g., Liu et al., 2014; Fig. 5), but there may be alternative explanations (other than toroidal flow) for this pattern, including the possibility of a lithospheric drip (West et al., 2009). It has proven difficult, however, to identify a compelling alternative explanation for the observations of anisotropy beneath the HLP region (Xue and Allen, 2006; Long et al., 2009; Wagner and Long, 2013). Beneath the HLP, the dense station coverage allows for the robust measurement of strong splitting with E-W fast orientations and delay times up to 2.5 s, with splitting parameters that do not appear to vary with azimuth, ruling out multiple layers of anisotropy (Long et al., 2009). These splitting observations are not easily reconciled with a two-dimensional corner flow model, which would predict fast orientations parallel to the Juan de Fuca-North America convergence direction, but match extremely well with the predictions for toroidal flow models that incorporate realistic kinematic parameters for Cascadia (Druken et al., 2011). This match between geodynamic model predictions and anisotropy observations, in combination with constraints from the timing and character of HLP and S/CRB volcanism (Ford et al., 2013; Till et al., 2013) and seismic tomography (Roth et al., 2008; James et al., 2011) led to the proposal of a conceptual model for mantle dynamics beneath the Pacific Northwest (Long et al., 2012), a cartoon of which is shown in Fig. 14. This conceptual model can explain many aspects of post-20 Ma volcanism in the Cascadia subduction zone (although it struggles to explain aspects of the Y/SRP volcanic trend; e.g., Camp, 2013; Foulger et al., 2015),

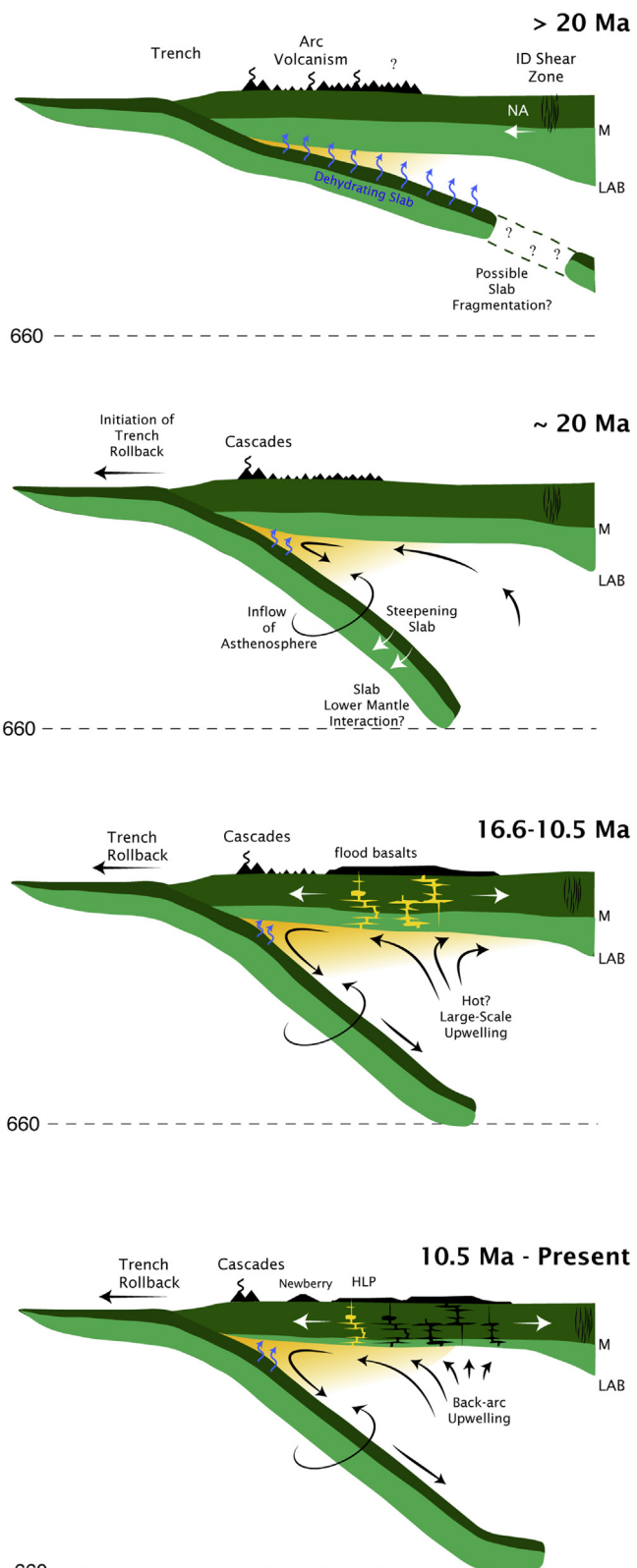


Fig. 14. Cartoon sketch of hypothesized mantle flow beneath the Pacific Northwest over the past ~20 Ma, reproduced from Long et al. (2012). Four time periods are shown, from top to bottom: pre-20 Ma, ~20 Ma (initiation of slab rollback), 16.6–10.5 Ma (S/CRB flood basalt era), and 10.5 Ma-present. The hypothesized present-day flow field includes a significant component of toroidal flow induced by slab rollback.

and can also explain a host of seismic, geochemical, and petrologic observables in the HLP region that are otherwise difficult to explain (Long et al., 2012). The most important implication of this model present-day mantle flow is that it requires the presence of a well-developed toroidal flow field induced by the rollback and steepening of the Juan de Fuca slab; it cannot be reconciled with a purely 2-D subduction-induced flow field, nor can it be easily reconciled with a highly fragmented slab in the upper mantle.

The morphology of the subducted Juan de Fuca slab at depth, and the extent to which it corresponds to a contiguous structure in the upper mantle that is capable of deflecting mantle flow in a toroidal pattern, is fundamental to understanding mantle flow beneath Cascadia. There is not yet consensus, however, on whether or not the slab is fragmented in the upper mantle, although there are robust arguments for complex, fragmented slab morphology in the mid-mantle portion of the subduction system. Taken together, tomographic images of the slab argue for some kind of fragmentation or at least along-strike variability of deep slab structure, but resolution is imperfect, and some authors have argued that the apparent slab window is an imaging artifact (Roth et al., 2008). Further complicating the issue, recent reflectivity imaging (Tauzin et al., 2016) is consistent with a continuous slab even in the portion of the system where tomographic imaging suggests a slab gap.

What is the role of the putative Yellowstone plume in our understanding of present-day mantle flow in the Cascadia subduction system? The existence, character, geometry, strength, and behavior of the Yellowstone plume, and its role in post-20 Ma volcanism in the Cascadia backarc, have been hotly debated (e.g., Fouch, 2012). Some workers have argued strenuously that the plume model is the best explanation for the S/CRB volcanism and the subsequent SRP trend (e.g., Camp and Ross, 2004; Smith et al., 2009; Camp, 2013; Kincaid et al., 2013) and that a plume that extends in depth to the lower mantle is imaged tomographically (e.g., Obrebski et al., 2010, 2011). Other workers have espoused models that emphasize subduction-related processes (e.g., Carlson and Hart, 1987; Long et al., 2012), pointed out the differences between tomographic images and the classical view of a simple mantle plume (e.g., James et al., 2011), highlighted the potential importance of lithospheric processes in producing PNW volcanism (e.g., Foulger et al., 2015), or emphasize the potential difficulties in models for plume-slab interaction (e.g., Leonard and Liu, 2016). The debate over the characteristics of the putative Yellowstone plume is far from settled; it is worth pointing out, however, that in the context of understanding the mantle flow field both in the present day and over the past ~20 Myr, it may not be a crucial question. A number of geodynamic modeling studies have pointed out that the flow field in the Cascadia subduction system is almost certainly controlled by subduction-related processes such as downdip motion of the slab and (potentially) slab rollback; if a plume is present, its behavior is likely controlled by the subduction-induced flow field (e.g. Kincaid et al., 2013; Leonard and Liu, 2016).

An interesting aspect of the Cascadia Paradox that remains to be explored in detail is whether and how the pattern of flow in the upper mantle interacts with patterns of crustal deformation on the overriding plate. One of the more robust geophysical observations that has emerged from recent work in the Pacific Northwest is the finding of a large-scale clockwise rotation of the PNW relative to North America (e.g., McCaffrey et al., 2000, 2007, 2013; Wells and McCaffrey (2016)). Rotation rates derived from GPS measurements generally match those inferred from paleomagnetic anomalies measured for the CRB, such that the present-day rotation agrees with the long-term rate over the past ~15 Ma (McCaffrey et al., 2013). As pointed out recently by McCaffrey et al. (2013), it is not immediately obvious how to reconcile the inference of generally E-W mantle flow beneath eastern Oregon (as suggested by shear wave splitting, and consistent with the idea of toroidal

flow) with the observed block rotation of the crust above it, unless there is mechanical decoupling between the crust and the asthenospheric mantle beneath it, or the crust is strong enough to resist deformation despite the application of basal tractions from mantle flow. Whether the mantle flow field in Cascadia is dominated by two-dimensional entrained flow or by three-dimensional toroidal flow, the question of how to reconcile mantle dynamics with crustal dynamics remains an exciting target for future research. The resolution of this question has important implications for our understanding of plate driving forces, the strength of the continental crust, and degree of mechanical coupling between plates and the underlying mantle.

How can we work towards resolving seemingly contradictory observations and come to a robust understanding of the pattern of mantle flow in the Cascadia subduction system and the forces that control that pattern? A resolution of the Cascadia Paradox will require a combination of constraints from observational seismology, geodynamic modeling, geochemistry, and geodesy, and the identification of new models that can provide explanations for seemingly contradictory inferences. There are a few directions for the near future that are likely to bear fruit. Of paramount importance is a better understanding of the morphology of the Juan de Fuca slab in the upper mantle and how that slab structure manifests itself in (imperfect) tomographic images. Tomographic inversions that take into account the known strong anisotropy in the PNW upper mantle may help to sharpen images of the slab (e.g., Bezada et al., 2016), and probabilistic inversions (e.g., Burdick and Lekic, 2015) may help to translate tomographically determined seismic wave speeds more directly into inferences about temperature and thus slab structure. On the geodynamic modeling side, continuing efforts to model mantle flow in subduction systems with a non-continuous (that is, fragmented) slab and to predict the anisotropy patterns that would result from such flow fields will be useful. Further geochemical investigations of possible along-strike flow in the Cascadia mantle wedge, building on the recent work of Mullen and Weis (2015), will be helpful, particularly in the southern portion of the subduction system.

From an observational seismology point of view, one critical aspect of anisotropic structure that has not yet been thoroughly addressed in the published literature is the possibility of depth-varying anisotropy beneath the offshore Juan de Fuca plate. A key argument against the large-scale toroidal flow model is the lack of evidence for a component of along-strike (that is, generally trench-parallel) return flow beneath the oceanic lithosphere of the Juan de Fuca plate. There is evidence in many other subduction systems for such flow from source-side splitting observations that sample the sub-slab mantle (e.g., Lynner and Long, 2014), but evidence from this type of measurement for Cascadia (Russo, 2009) is mixed. SKS splitting measurements for Cascadia Initiative OBS stations do not show evidence for the significant component of trench-parallel flow that would be expected for the large-scale toroidal flow model. However, the short deployment times and high noise level associated with OBS instrumentation mean that the azimuthal coverage for SKS splitting is poor, and the measurements of Bodmer et al. (2015) and Martin-Short et al. (2015) are unlikely to be sensitive to multiple layers of anisotropy. If the return flow associated with a toroidal flow field is accommodated in the deeper portions of the upper mantle beneath the Juan de Fuca oceanic plate, with a shallower layer of anisotropy due to plate motion parallel shearing, then this may not be obvious from SKS splitting. Surface wave models derived from Cascadia Initiative data that include the possibility of multiple layers of anisotropy may be crucial for resolving this point.

Another avenue for future investigation that may prove fruitful is the re-evaluation of the suite of seismic, geodynamic, petrologic, and geochemical observations from the recent High Lava

Plains project in the eastern Oregon backarc. The synthesis of Long et al. (2012) argued that these observations are best explained by a model that invokes toroidal flow driven by the rollback and steepening of the Cascadia slab. However, as discussed in this paper, it is difficult to reconcile this model with the increasingly convincing evidence for some type of fragmentation of the Cascadia slab at depth, or with the two-dimensional entrained flow that is suggested by anisotropy data in other portions of the system. No convincing alternative explanation for the strong anisotropy with E-W fast orientations and large delay times observed beneath the HLP region has yet been investigated in detail; however, the identification and evaluation of alternative models for mantle flow beneath the HLP is important.

Because of the extensive data collection that has been done in the central and southern portions of Cascadia as part of EarthScope, GeoPRISMS, the Cascadia Initiative, and related efforts, most studies of mantle flow have focused on the central and southern part of the subduction system. However, intriguing results have also been obtained near its northern edge, where the Explorer microplate subducts beneath North America and the margin transitions from subduction to transform motion going from south to north (Fig. 1). These include shear wave splitting observations that suggest a significant departure from two-dimensional entrained flow (Mosher et al., 2014) as well as seismic imaging studies that have suggested a complex and evolving slab morphology, with likely toroidal flow around its edge (e.g., Audet et al., 2008; Mercier et al., 2009). Using geochemical tools, Thorkelson et al. (2011) identified evidence for upwelling-induced melting and volcanism to the north of the slab edge, implying that large-scale mantle flow has been controlled by the temporal evolution of the slab at depth. Future investigations of the slab morphology and the mantle flow regime at the northern edge of the Cascadia subduction system should yield important insight that is complementary to the extensive investigations that have been done in its central and southern portions.

Finally, analogies with other subduction systems should be considered as a potential source of future insight into the dynamics of the Cascadia subduction system. There is a natural analogy with the Mexican subduction zone, where the Cocos and Rivera slabs (like the Juan de Fuca, remnants of the ancient Farallon plate; Severinghaus and Atwater, 1990) subduct beneath Mexico. Like Cascadia, this subduction system is undergoing rollback (e.g., Ferrari et al., 2001), and as with Cascadia, the flow field seems to combine elements of both the 2D entrained flow and 3D toroidal flow scenarios, based on anisotropy observations (León Soto et al., 2009; Stublai et al., 2012). There may also be one or more slab gaps or tears in the slab beneath Mexico (e.g., Dougherty and Clayton, 2014), so this system may provide another example of how a fragmented slab interacts with the mantle around it to drive flow. Future investigations that compare and contrast the slab morphology, subduction kinematics, volcanic patterns and chemistry, and seismic anisotropy of the Mexican and Cascadia subduction zones may well produce new insights into what factors control the mantle flow fields in these analogous systems.

7. Conclusions

Despite extensive study, the pattern of mantle flow associated with the Cascadia subduction system remains poorly understood. Two different endmember models – the two-dimensional entrained flow model and the large-scale three-dimensional toroidal flow model – are commonly invoked to explain geophysical, geochemical, petrologic, and other observations. However, there is as yet no consensus on either the pattern of mantle flow or the drivers of the flow field. It is likely that the actual flow field reflects a combination of processes, with neither end-member

model providing a complete description of flow; for example, large-scale three-dimensional toroidal flow may co-exist with a layer of entrained flow directly beneath the slab. Different types of seismic anisotropy observations in different portions of the system argue for different flow regimes, and reconciling these different interpretations is of critical importance. Specifically, observations in the backarc portion of the overriding plate seem to favor a toroidal flow model, while offshore observations on the downgoing plate favor entrained flow. There is convincing evidence from both seismic anisotropy and geochemical observations for at least some contribution from three-dimensional flow in the immediate vicinity of the slab edges, but it remains unclear whether a large-scale toroidal flow field is present.

The detailed morphology of the subducted Juan de Fuca slab at depth is intimately related to the question of the mantle flow field. Large-scale toroidal flow requires that the slab be intact enough to deflect flow around the slab sides as the slab rolls back. However, recent tomographic imaging using new data from the Transportable Array and Cascadia Initiative suggests that the slab may be fragmented in the upper mantle, casting doubt on the toroidal flow model. Resolution of tomographic models is imperfect, however, and results from reflectivity imaging suggests the presence of a continuous slab in the upper mantle. Resolution of the Cascadia Paradox will require tighter constraints on the actual morphology of the slab at depth, new models for seismic anisotropy throughout the upper mantle that include the possibility of multiple layers (particularly in the offshore portions of the system), further analysis of geochemical tracers, and further geodynamic modeling studies that examine the effects of more realistic slab morphologies on mantle flow.

Acknowledgements

I am grateful for stimulating discussions on the dynamics of the Cascadia subduction system with many colleagues and collaborators, particularly fellow participants in the High Lava Plains Project. I thank Timothy Horscroft for the invitation to write this paper. Richard Allen, Miles Bodmer, Kelsey Druken, Caroline Eakin, Haiying Gao, Robert Martin-Short, Emily Mullen, Benoit Tauzin, Christy Till, Lara Wagner, and Dominique Weis graciously provided figure files. Images from Ed Garnero (<http://garnero.asu.edu>) were helpful in drafting Fig. 4. Figures from *Geology*, *Nature Geoscience*, *Geophysical Journal International*, *Earth and Planetary Science Letters*, *Geophysical Research Letters*, and *Geochemistry, Geophysics, Geosystems* were reproduced with permission. GeoMapApp, the Matlab Mapping Toolbox, and the Generic Mapping Tools were used to generate figures. I thank Raúl Valenzuela and two anonymous reviewers for constructive comments that helped to improve the paper. This work was supported in part by NSF grant EAR-1150722.

References

- Audet, P., Bostock, M.G., Mercier, J.-P., Cassidy, J.F., 2008. Morphology of the Explorer-Juan de Fuca slab edge in northern Cascadia: imaging plate capture at a ridge-trench-transform triple junction. *Geology* 36, 895–898, <http://dx.doi.org/10.1130/G25356A.1>.
- Balfour, N.J., Cassidy, J.F., Dosso, S.E., 2012. Crustal anisotropy in the forearc of the northern Cascadia subduction zone, British Columbia. *Geophys. J. Int.* 188, 165–176, <http://dx.doi.org/10.1111/j.1365-246X.2011.05231.x>.
- Becker, T.W., 2012. On recent seismic tomography for the western United States. *Geochem. Geophys. Geosyst.* 13, <http://dx.doi.org/10.1029/2011gc003977>, Q01W10.
- Beghein, C., Snoker, J.A., Fouch, M.J., 2010. Depth constraints on azimuthal anisotropy in the Great Basin from Rayleigh wave phase velocity maps. *Earth Planet. Sci. Lett.* 289, 467–478, <http://dx.doi.org/10.1016/j.epsl.2009.11.036>.
- Bezada, M.J., Faccenda, M., Toomey, D.R., 2016. Representing anisotropic subduction zones with isotropic velocity models: a characterization of the problem and some steps on a possible path forward. *Geochem. Geophys. Geosyst.* 17, <http://dx.doi.org/10.1002/2016gc006507>.

- Billen, M.I., 2008. Modeling the dynamics of subducting slabs. *Annu. Rev. Earth Planet. Sci.* 36, 325–356.
- Bodmer, M., Toomey, D.R., Hooft, E.E., Nábělek, J., Braunmiller, J., 2015. Seismic anisotropy beneath the Juan de Fuca plate system: evidence for heterogeneous mantle flow. *Geology* 43, 1095–1098, <http://dx.doi.org/10.1130/G37181.1>.
- Boneh, Y., Morales, L.F.G., Kaminski, E., Skemer, P., 2015. Modeling olivine CPO evolution with complex deformation histories—implications for the interpretation of seismic anisotropy in the mantle. *Geochim. Geophys. Geosyst.* 16, <http://dx.doi.org/10.1002/2-15GC005964>.
- Bostock, M.G., Cassidy, J.F., 1995. Variations in SKS splitting across western Canada. *Geophys. Res. Lett.* 22, 5–8, <http://dx.doi.org/10.1029/94GL02789>.
- Bostock, M.G., Christensen, N.I., 2012. Split from slip and schist: crustal anisotropy beneath northern Cascadia from non-volcanic tremor. *J. Geophys. Res.* 117, <http://dx.doi.org/10.1029/2011jb009095>, B08303.
- Bostock, M.G., Hyndman, R.D., Rondenay, S., Peacock, S.M., 2002. An inverted continental Moho and serpentinization of the forearc mantle. *Nature* 417, 536–538, <http://dx.doi.org/10.1038/417536a>.
- Buehler, J.S., Shearer, P.M., 2010. Pn tomography of the western United States using USArray. *J. Geophys. Res.* 115, <http://dx.doi.org/10.1029/2009jb006874>, B09315.
- Burdick, S., Lekic, V., 2015. Investigating the Farallon slab with probabilistic traveltime tomography. *AGU Fall Meeting Abstract*, T24A-04.
- Buttles, J., Olson, P., 1998. A laboratory model of subduction zone anisotropy. *Earth Planet. Sci. Lett.* 164, 245–262.
- Camp, V.E., Hanan, B.B., 2008. A plume-triggered delamination origin for the Columbia River Basalt Group. *Geosphere* 4, 480–496, <http://dx.doi.org/10.1130/GES00175.1>.
- Camp, V.E., Ross, M.E., 2004. Mantle dynamics and genesis of mafic magmatism in the intermontane Pacific Northwest. *J. Geophys. Res.* 109, <http://dx.doi.org/10.1029/2003jb002838>, B08204.
- Camp, V.E., 2013. Origin of Columbia River Basalt: Passive rise of shallow mantle, or active upwelling of a deep-mantle plume? Origin of Columbia River Basalt: passive rise of shallow mantle, or active upwelling of a deep-mantle plume? *Geol. Soc. Am. Spec. Pap.*, 497, 181–199.
- Carlson, R.W., Hart, W.K., 1987. Crustal genesis on the Oregon Plateau. *J. Geophys. Res.* 92, 6191–6206, <http://dx.doi.org/10.1029/JB092iB07p06191>.
- Chen, C., Zhao, D., Wu, S., 2015. Tomographic imaging of the Cascadia subduction zone: constraints on the Juan de Fuca slab. *Tectonophysics* 647–648, 73–88.
- Chen, Z., Schellart, W.P., Strak, V., Duarte, J.C., 2016. Does subduction-induced mantle flow drive backarc extension? *Earth Planet. Sci. Lett.* 441, 200–210.
- Chu, R., Schmandt, B., Helmberger, D.V., 2012. Juan de Fuca subduction zone from a mixture of tomography and waveform modeling. *J. Geophys. Res.* 117, <http://dx.doi.org/10.1029/2012jb009146>, B03304.
- Crankin, S., 1981. A review of wave motion in anisotropic and cracked elastic-media. *Wave Motion* 3, 343–391.
- Currie, C.A., Cassidy, J.F., Hyndman, R.D., 2001. A regional study of shear wave splitting above the Cascadia Subduction Zone: margin-parallel crustal stress. *Geophys. Res. Lett.* 28, 659–662, <http://dx.doi.org/10.1029/2000GL011978>.
- Currie, C.A., Cassidy, J.F., Hyndman, R.D., Bostock, M.G., 2004. Shear wave anisotropy beneath the Cascadia subduction zone and western North American craton. *Geophys. J. Int.* 157, 341–353, <http://dx.doi.org/10.1111/j.1365-246X.2004.02175.x>.
- Darold, A., Humphreys, E., 2013. Upper mantle seismic structure beneath the Pacific Northwest: a plume-triggered delamination origin for the Columbia River flood basalts. *Earth Planet. Sci. Lett.* 365, 232–242.
- Dougherty, S.L., Clayton, R.W., 2014. Seismicity and structure in central Mexico: evidence for a possible slab tear in the South Cocos plate. *J. Geophys. Res.* 119, 3424–3447, <http://dx.doi.org/10.1020/2013JB010833>.
- Druken, K.A., Long, M.D., Kincaid, C., 2011. Patterns in seismic anisotropy driven by rollback subduction beneath the High Lava Plains. *Geophys. Res. Lett.* 38, <http://dx.doi.org/10.1029/2011gl047541>, L13310.
- Eagar, K.C., Fouch, M.J., James, D.E., Carlson, R.W., 2011. Crustal structure beneath the High Lava Plains of eastern Oregon and surrounding regions from receiver function analysis. *J. Geophys. Res.* 116, <http://dx.doi.org/10.1029/2010jb007795>, B02313.
- Eakin, C.M., Obrebski, M., Allen, R.M., Boyarko, D.C., Brudzinski, M.R., Porritt, R., 2010. Seismic anisotropy beneath Cascadia and the Mendocino triple junction: interaction of the subducting slab with mantle flow. *Earth Planet. Sci. Lett.* 297, 627–632, <http://dx.doi.org/10.1016/j.epsl.2010.07.015>.
- Evans, M.S., Kendall, J.-M., Willmann, R.J., 2006. Automated SKS splitting and upper-mantle anisotropy beneath Canadian seismic stations. *Geophys. J. Int.* 165, 931–942.
- Fabritius, R.A., 1995. Shear-wave Anisotropy Across the Cascade Subduction Zone from a Linear Seismograph Array. M.S Thesis. Oregon State University.
- Faccenda, M., Capitanio, F.A., 2013. Seismic anisotropy around subduction zones: insights from three-dimensional modeling of upper mantle deformation and SKS splitting calculations. *Geochim. Geophys. Geosyst.* 14, 243–262, <http://dx.doi.org/10.1002/ggge.20055>.
- Faccenna, C., Bekker, T.W., Lallemand, S., Lagabrielle, Y., Funiciello, F., Piromallo, C., 2010. Subduction-triggered magmatic pulses: a new class of plumes? *Earth Planet. Sci. Lett.* 299, 54–68, <http://dx.doi.org/10.1016/j.epsl.2010.08.012>.
- Ferrari, L., Petrone, C.M., Francalanci, L., 2001. Generation of ocean-island basalt-type volcanism in the western Trans-Mexican volcanic belt by slab rollback, asthenosphere infiltration, and variable flux melting. *Geology* 29, 507–510.
- Ford, M.T., Grunder, A.L., Duncan, R.A., 2013. Bimodal volcanism of the High Lava Plains and northwestern Basin and Range of Oregon: distribution and tectonic implications of age-progressive rhyolites. *Geochem. Geophys. Geosyst.* 14, 2836–2857, <http://dx.doi.org/10.1002/ggge.20175>.
- Fouch, M.J., West, J.D., 2008. High resolution imaging of the mantle flow field beneath western North America. *Eos Trans. AGU*, 89(53), Fall Meet. Suppl., Abstract U53C-06.
- Fouch, M.J., 2012. The Yellowstone hotspot: plume or not? *Geology* 40, 479–480, <http://dx.doi.org/10.1130/focus052012.1>.
- Foulger, G.R., Christiansen, R.L., Anderson, D.L., 2015. The Yellowstone hot spot track results from migrating basin-range extension. In: Foulger, G.R., Lustro, M., King, S.D. (Eds.), *The Interdisciplinary Earth: A Volume in Honor of Don L. Anderson*, vol. 514. *Geol. Soc. Am.*, [http://dx.doi.org/10.1130/2015.2514\(14\).Spec.Pap](http://dx.doi.org/10.1130/2015.2514(14).Spec.Pap).
- Gao, H., Shen, Y., 2014. Upper mantle structure of the Cascades from full-wave ambient noise tomography: evidence for 3D mantle upwelling in the back-arc. *Earth Planet. Sci. Lett.* 390, 222–233.
- Geist, D., Richards, M., 1993. Origin of the Columbia Plateau and Snake River Plain: deflection of the Yellowstone plume. *Geology* 21, 789–792.
- Gerya, T., 2011. Future directions in subduction modeling. *J. Geodyn.* 52, 344–378.
- Goldfinger, C., Nelson, C.H., Johnson, J.E., 2003. Holocene earthquake records from the Cascadia subduction zone and northern San Andreas fault based on precise dating of offshore turbidites. *Annu. Rev. Earth Planet. Sci.* 31, 555–577.
- Hanson-Hedcock, S., Wagner, L.S., Fouch, M.J., James, D.E., 2012. Constraints on the causes of mid-Miocene volcanism in the Pacific Northwest US from ambient noise tomography. *Geophys. Res. Lett.* 39, <http://dx.doi.org/10.1029/2012gl051108>, L05301.
- Heuret, A., Lallemand, S., 2005. Plate motions, slab dynamics and back-arc deformation. *Phys. Earth Planet. Inter.* 149, 31–51, <http://dx.doi.org/10.1016/j.pepi.2004.08.022>.
- Hoernle, K., Abt, D.L., Fischer, K.M., Nichols, H., Hauff, F., Abers, G.A., van der Bogaard, P., Heydolph, K., Alvarado, G., Protti, M., Strauch, W., 2008. Geochemical and geophysical evidence for arc-parallel flow in the mantle wedge beneath Costa Rica and Nicaragua. *Nature* 451, 1094–1098.
- Huang, Z., Zhao, D., 2013. Mapping P wave azimuthal anisotropy in the crust and upper mantle beneath the United States. *Phys. Earth Planet. Inter.* 225, 28–40.
- Jadamec, M.A., 2016. Insights on slab-driven mantle flow from advances in three-dimensional modelling. *J. Geodyn.* 100, 51–70.
- James, D.E., Fouch, M.J., Carlson, R.W., Roth, J.B., 2011. Slab fragmentation, edge flow and the origin of the Yellowstone hotspot track. *Earth Planet. Sci. Lett.* 311, 124–135.
- Jordan, B.T., 2005. Age-progressive volcanism of the Oregon High Lava Plains: Overview and evaluation of tectonic. *Geol. Soc. Am. Spec. Pap.*, 388, 503–515.
- Jung, H., Karato, S.-i., 2001. Water-induced fabric transitions in olivine. *Science* 293, 1460–1463.
- Jung, H., Katayama, I., Jiang, Z., Hiraga, T., Karato, S., 2006. Effect of water and stress on the lattice preferred orientation (LPO) of olivine. *Tectonophysics* 421, 1–22.
- Jung, H., 2011. Seismic anisotropy produced by serpentine in mantle wedge. *Earth Planet. Sci. Lett.* 307, 535–543.
- Karato, S.-i., Jung, H., Katayama, I., Skemer, P., 2008. Geodynamic significance of seismic anisotropy of the upper mantle: new insights from laboratory studies. *Annu. Rev. Earth Planet. Sci.* 36, 59–95.
- Katayama, I., Kirauchi, K.-I., Michibayashi, K., Ando, J.-I., 2009. Trench-parallel anisotropy produced by serpentine deformation in the hydrated mantle wedge. *Nature* 461, 1114–1117.
- Kincaid, C., Druken, K.A., Griffiths, R.W., Stegman, D.R., 2013. Bifurcation of the Yellowstone plume driven by subduction-induced mantle flow. *Nat. Geosci.* 6, 395–399.
- Kneller, E.A., van Keeken, P.E., Karato, S., Park, J., 2005. B-type olivine fabric in the mantle wedge: insights from high-resolution non-Newtonian subduction zone models. *Earth Planet. Sci. Lett.* 237, 781–797.
- León Soto, G.L., Ni, J.F., Grand, S.P., Sandvol, E., Valenzuela, R.W., Guzmán Speziale, M., Gómez González, J.M., Domínguez Reyes, T., 2009. Mantle flow in the Rivera-Cocos subduction zone. *Geophys. J. Int.* 179, 1004–1012, <http://dx.doi.org/10.1111/j.1365-0246.2009.04352.x>.
- Leeman, W.P., Annen, C., Dufek, J., 2008. Snake River Plain–Yellowstone silicic volcanism: implications for magma genesis and magma fluxes. In: Annen, C., Zellmer, G.F. (Eds.), *Dynamics of Crustal Magma Transfer, Storage and Differentiation*, vol. 304. *Geol. Soc. London Spec. Pub.*, pp. 235–259.
- Leonard, T., Liu, L., 2016. The role of a mantle plume in the formation of Yellowstone volcanism. *Geophys. Res. Lett.* 43, <http://dx.doi.org/10.1002/2015gl067131>.
- Levin, V., Okaya, D., Park, J., 2007a. Shear wave birefringence in wedge-shaped anisotropic regions. *Geophys. J. Int.* 168, 275–286.
- Levin, V., Park, J., Lucente, F.P., Margheriti, L., Pondrelli, S., 2007b. End of subduction in northern Apennines confirmed by observations of quasi-Love waves from the great 2004 Sumatra-Andaman earthquake. *Geophys. Res. Lett.* 34, L04304, <http://dx.doi.org/10.1029/2006GL028860>.
- Lin, F.-C., Ritzwoller, M.H., Yang, Y., Moschetti, M.P., Fouch, M.J., 2011. Complex and variable crustal and uppermost mantle seismic anisotropy in the western United States. *Nat. Geosci.* 4, 55–61.
- Liu, L., Stegman, D.R., 2012. Origin of Columbia River flood basalts controlled by propagating rupture of the Farallon slab. *Nature* 482, 386–389.
- Liu, K., Elsheik, A., Lemnifi, A., Purevasuren, U., Ray, M., Refayee, H., Yang, B., Yu, Y., Gao, S.S., 2014. A uniform database of teleseismic shear wave splitting

- measurements for the western and central United States. *Geochem. Geophys. Geosyst.* 15, 2075–2085, <http://dx.doi.org/10.1002/2014GC005267>.
- Li, Z.-H., Di Leo, J.F., Ribe, N.M., 2014. Subduction-induced mantle flow, finite strain, and seismic anisotropy: numerical modeling. *J. Geophys. Res. Solid Earth* 119, 5052–5076, <http://dx.doi.org/10.1002/2014JB010996>.
- Long, M.D., Becker, T.W., 2010. Mantle dynamics and seismic anisotropy. *Earth Planet. Sci. Lett.* 297, 341–354.
- Long, M.D., Silver, P.G., 2008. The subduction zone flow field from seismic anisotropy: a global view. *Science* 319, 315–318.
- Long, M.D., Silver, P.G., 2009. Mantle flow in subduction systems: the subslab flow field and implications for mantle dynamics. *J. Geophys. Res.* 114, <http://dx.doi.org/10.1029/2008jb006200>, B10312.
- Long, M.D., Gao, H., Klaus, A., Wagner, L.S., Fouch, M.J., James, D.E., Humphreys, E., 2009. Shear wave splitting and the pattern of mantle flow beneath eastern Oregon. *Earth Planet. Sci. Lett.* 288, 359–369.
- Long, M.D., Till, C.B., Druken, K.A., Carlson, R.W., Wagner, L.S., Fouch, M.J., James, D.E., Grove, T.L., Schmerr, N., Kincaid, C., 2012. Mantle dynamics beneath the Pacific Northwest and the generation of voluminous back-arc volcanism. *Geochem. Geophys. Geosyst.* 13, <http://dx.doi.org/10.1029/2012gc004189>, Q0AN01.
- Long, M.D., Biryol, C.B., Eakin, C.M., Beck, S.L., Wagner, L.S., Zandt, G., Minaya, E., Tavera, H., 2016. Overriding plate, mantle wedge, slab, and subslab contributions to seismic anisotropy beneath the northern Central Andean Plateau. *Geochem. Geophys. Geosyst.* 17, 2556–2575, <http://dx.doi.org/10.1029/2016GC006316>.
- Long, M.D., 2013. Constraints on subduction geodynamics from seismic anisotropy. *Rev. Geophys.* 51, 76–112, <http://dx.doi.org/10.1002/rog.20008>.
- Lynner, C., Long, M.D., 2014. Sub-slab anisotropy beneath the Sumatra and circum-Pacific subduction zones from source-side shear wave splitting observations. *Geochem. Geophys. Geosyst.* 15, 2262–2281, <http://dx.doi.org/10.1029/2014GC005239>.
- MacDougall, J.G., Kincaid, C., Szwaia, S., Fischer, K.M., 2014. The impact of slab dip variations, gaps and rollback on mantle wedge flow: insights from fluids experiments. *Geophys. J. Int.* 197, 705–730.
- Martin-Short, R., Allen, R.M., Bastow, I.D., Totten, E., Richards, M.A., 2015. Mantle flow geometry from ridge to trench beneath the Gorda-Juan de Fuca plate system. *Nat. Geosci.* 8, 965–968.
- McCaffrey, R., Long, M.D., Goldfinger, C., Zwick, P.C., Nabelek, J.L., Johnson, C.K., Smith, C., 2000. Rotation and plate locking at the southern Cascadia subduction zone. *Geophys. Res. Lett.* 27, 3117–3120, <http://dx.doi.org/10.1029/2000GL011768>.
- McCaffrey, R., Qamar, A.I., King, R.W., Wells, R., Khazadze, G., Williams, C.A., Stevens, C.W., Vollck, J.J., Zwick, P.C., 2007. Fault locking, block rotation and crustal deformation in the Pacific Northwest. *Geophys. J. Int.* 169, 1315–1340.
- McCaffrey, R., King, R.W., Payne, S.J., Lancaster, M., 2013. Active tectonics of northwestern U.S. inferred from GPS-derived surface velocities. *J. Geophys. Res.* 118, 1–15, <http://dx.doi.org/10.1029/2012JB009473>.
- McCrory, P.A., Blair, J.L., Waldhauser, F., Oppenheimer, D.H., 2012. Juan de Fuca slab geometry and its relation to Watari-Benioff zone seismicity. *J. Geophys. Res.* 117, <http://dx.doi.org/10.1029/2012JB009407>, B09306.
- Mercier, J.-P., Bostock, M.G., Cassidy, J.F., Dueker, K., Gaherty, J.B., Garner, E.J., Revenaugh, J., Zandt, G., 2009. Body-wave tomography of western Canada. *Tectonophysics* 475, 480–492, <http://dx.doi.org/10.1016/j.tecto.2009.05.030>.
- Mosher, S.G., Audet, P., L'Heureux, I., 2014. Seismic evidence for rotating mantle flow around subducting slab edge associated with oceanic microplate capture. *Geophys. Res. Lett.* 41, 4548–4553, <http://dx.doi.org/10.1002/2014GL060630>.
- Mullen, E.K., Weis, D., 2015. Evidence for trench-parallel mantle flow in the northern Cascade Arc from basalt geochemistry. *Earth Planet. Sci. Lett.* 414, 100–107.
- Nikulin, A., Levin, V., Park, J., 2009. Receiver function study of the Cascadia megathrust: evidence for localized serpentinization. *Geochem. Geophys. Geosyst.* 10, <http://dx.doi.org/10.1029/2009gc002376>, Q07004.
- Obrebski, M., Allen, R.M., Xue, M., Hung, S., 2010. Slab-plume interaction beneath the Pacific Northwest. *Geophys. Res. Lett.* 37, <http://dx.doi.org/10.1029/2010gl043489> (L14305).
- Obrebski, M., Allen, R.M., Pollitz, F., Hung, S.-H., 2011. Lithosphere–asthenosphere interaction beneath the western United States from the joint inversion of body-wave traveltimes and surface-wave phase velocities. *Geophys. J. Int.* 185, 1003–1021.
- Paczkowski, K., Montési, L.G.J., Long, M.D., Thissen, C.J., 2014. Three-dimensional flow in the subslab mantle. *Geochem. Geophys. Geosyst.* 15, 3989–4008, <http://dx.doi.org/10.1029/2014GC005441>.
- Park, J., Yuan, H., Levin, V., 2004. Subduction zone anisotropy beneath Corvallis, Oregon: a serpentinite skid mark of trench-parallel terrane migration? *J. Geophys. Res.* 109, <http://dx.doi.org/10.1029/2003jb002718>, B10306.
- Pavlis, G.L., Sigloch, K., Burdick, S., Fouch, M.J., Vernon, F.L., 2012. Unraveling the geometry of the Farallon plate: synthesis of three-dimensional imaging results from US Array. *Tectonophysics* 532–535, 82–102.
- Peyton, V., Levin, V., Park, J., Brandon, M., Lees, J., Gordeev, E., Ozerov, A., 2001. Mantle flow at a slab edge: seismic anisotropy in the Kamchatka region. *Geophys. Res. Lett.* 28, 379–382.
- Piromallo, C., Becker, T.W., Funiciello, F., Fannenna, C., 2006. Three-dimensional instantaneous mantle flow induced by subduction. *Geophys. Res. Lett.* 33, <http://dx.doi.org/10.1029/2005gl025390>, L08304.
- Porritt, R.W., Allen, R.M., Boyarko, D.C., Brudzinski, M.R., 2011. Investigation of Cascadia segmentation with ambient noise tomography. *Earth Planet. Sci. Lett.* 309, 67–76, <http://dx.doi.org/10.1016/j.epsl.2011.06.026>.
- Rieger, D.M., Park, J., 2010. USArray observations of quasi-love surface wave scattering: orienting anisotropy in the Cascadia plate boundary. *J. Geophys. Res.* 115, <http://dx.doi.org/10.1029/2009jb006754>, B05306.
- Roth, J.B., Fouch, M.J., James, D.E., Carlson, R.W., 2008. Three-dimensional seismic velocity structure of the northwestern United States. *Geophys. Res. Lett.* 35, <http://dx.doi.org/10.1029/2008GL03466>, L15304.
- Russo, R.M., Silver, P.G., 1994. Trench-parallel flow beneath the Nazca plate from seismic anisotropy. *Science* 263, 1105–1111.
- Russo, R.M., 2009. Subducted oceanic asthenosphere and upper mantle flow beneath the Juan de Fuca slab. *Lithosphere* 1, 195–205.
- Savage, M.D., Sheehan, A.F., 2000. Seismic anisotropy and mantle flow from the Great Basin to the Great Plains, western United States. *J. Geophys. Res.* 105, 13715–13734, <http://dx.doi.org/10.1029/2000JB900021>.
- Savage, M.K., 1999. Seismic anisotropy and mantle deformation: what have we learned from shear wave splitting? *Rev. Geophys.* 37, 65–106.
- Schellart, W.P., Strak, V., 2016. A review of analogue modelling of geodynamic processes: approaches, scaling, materials and quantification, with an application to subduction experiments. *J. Geodyn.* 100, 7–32, <http://dx.doi.org/10.1016/j.jog.2016.03.009>.
- Schellart, W.P., Freeman, J., Stegman, D.R., Moresi, L., May, D., 2007. Evolution and diversity of subduction zones controlled by slab width. *Nature* 446, 308–311.
- Schellart, W.P., Stegman, D.R., Freeman, J., 2008. Global trench migration velocities and slab migration induced upper mantle volume fluxes: constraints to find an Earth reference frame based on minimizing viscous dissipation. *Earth Sci. Rev.* 88, 118–144.
- Schellart, W.P., Stegman, D.R., Farrington, R.J., Freeman, J., Moresi, L., 2010. Cenozoic tectonics of Western North America controlled by evolving width of Farallon slab. *Science* 329, 316–319.
- Schellart, W.P., 2010. Mount Etna-Iblean volcanism caused by rollback-induced upper mantle upwelling around the Ionian slab edge: an alternative to the plume model. *Geology* 38, 691.
- Schmandt, B., Humphreys, E.D., 2010. Complex subduction and small-scale convection revealed by body wave tomography of the western U.S. upper mantle. *Earth Planet. Sci. Lett.* 297, 435–445.
- Schutt, D., Humphreys, E.D., Dueker, K., 1998. Anisotropy of the Yellowstone hot spot wake, Eastern Snake River Plain, Idaho. *Pure Appl. Geophys.* 151, 443–462.
- Severinghaus, J., Atwater, T., 1990. Cenozoic geometry and thermal state of the subducting slabs beneath North America. In: Wernicke, B.P. (Ed.), *Basin and Range Extensional Tectonics Near the Latitude of Las Vegas Nevada*, vol. 176. Mem. Geol. Soc. Am., pp. 1–22.
- Sigloch, K., 2011. Mantle provinces under North America from multifrequency P wave tomography. *Geochem. Geophys. Geosyst.* 12, <http://dx.doi.org/10.1029/2010gc003421>, Q02W08.
- Silver, P.G., 1996. Seismic anisotropy beneath the continents: probing the depths of geology. *Annu. Rev. Earth Planet. Sci.* 24, 385–432.
- Skemer, P., Hansen, L.N., 2016. Inferring upper-mantle flow from seismic anisotropy: an experimental perspective. *Tectonophysics* 668–669, 1–14.
- Smith, R.B., Jordan, M., Steinberger, B., Puskas, C.M., Farrell, J., Waite, G.P., Husen, S., Chang, W.-L., O'Connell, R., 2009. Geodynamics of the Yellowstone hotspot and mantle plume: seismic and GPS imaging, kinematics, and mantle flow. *J. Volcanol. Geotherm. Res.* 188, 26–56.
- Song, T.-R.A., Kawakatsu, H., 2012. Subduction of oceanic asthenosphere: evidence from sub-slab seismic anisotropy. *Geophys. Res. Lett.* 39, <http://dx.doi.org/10.1029/2012gl052639>, L17301.
- Strak, V., Schellart, W.P., 2014. Evolution of 3-D subduction-induced mantle flow around lateral slab edges in analogue models of free subduction analysed by stereoscopic particle image velocimetry technique. *Earth Planet. Sci. Lett.* 403, 368–379.
- Strak, V., Schellart, W.P., 2016. Control of slab width on subduction-induced upper mantle flow and associated upwellings: insights from analog models. *J. Geophys. Res.* 121, <http://dx.doi.org/10.1002/2015jb012545>.
- Stubailo, I., Beghein, C., Davis, P.M., 2012. Structure and anisotropy of the Mexico subduction zone based on Rayleigh-wave analysis and implications for the geometry of the Trans-Mexican Volcanic Belt. *J. Geophys. Res.* 117, <http://dx.doi.org/10.1029/2011jb008631>, B05303.
- Tauzin, B., Bodin, T., Debayle, E., Perrillat, J.-P., Reynard, B., 2016. Multi-mode conversion imaging of the subducted Gorda and Juan de Fuca plates below the North American continent. *Earth Planet. Sci. Lett.* 440, 135–146.
- Thorkelson, D.J., Madsen, J.K., Sluggett, C.L., 2011. Mantle flow through the Northern Cordilleran slab window revealed by volcanic geochemistry. *Geology* 39, 267–270, <http://dx.doi.org/10.1130/G31522.1>.
- Till, C.B., Grove, T.L., Carlson, R.W., Donnelly-Nolan, J.M., Fouch, M.J., Wagner, L.S., Hart, W.K., 2013. Depths and temperatures of <10.5 Ma mantle melting and the lithosphere–asthenosphere boundary below southern Oregon and northern California. *Geochem. Geophys. Geosyst.* 14, <http://dx.doi.org/10.1002/ggge.20070>.
- Toomey, D.R., Allen, R.M., Barclay, A.H., bell, S.W., Bromirski, P.D., Carlson, R.L., Chen, X., Collins, J.A., Dziak, R.P., Evers, B., Forsyth, D.W., Gerstoft, P., Hoof, E.E., Livelybrooks, D., Lodewyk, J.A., Luther, D.S., McGuire, J.J., Schwartz, S.Y., Tolstoy, M., Tréhu, A.M., Weirathmueller, M., Wilcock, W.S.D., 2014. The Cascadia Initiative: a sea change in seismological studies of subduction zones. *Oceanography* 27, 138–150.

- Turner, S., Hawkesworth, C., 1998. Using geochemistry to map mantle flow beneath the Lau Basin. *Geology* 26, 1019–1022.
- Wagner, L.S., Long, M.D., 2013. Distinctive upper mantle anisotropy beneath the High Lava Plains and Eastern Snake River Plain, Pacific Northwest, USA. *Geochem. Geophys. Geosyst.* 14, 4647–4666, <http://dx.doi.org/10.1002/ggge.20275>.
- Wagner, L.S., Forsyth, D.W., Fouch, M.J., James, D.E., 2010. Detailed three-dimensional shear wave velocity structure of the northwestern United States from Rayleigh wave tomography. *Earth Planet. Sci. Lett.* 299, 273–284.
- Wagner, L.S., Fouch, M.J., James, D.E., Long, M.D., 2013. The role of hydrous phases in the formation of trench parallel anisotropy: evidence from Rayleigh waves in Cascadia. *Geophys. Res. Lett.*, <http://dx.doi.org/10.1002/grl.50525>.
- Waite, G.P., Schutt, D.L., Smith, R.B., 2005. Models of lithosphere and asthenosphere anisotropic structure of the Yellowstone hot spot from shear wave splitting. *J. Geophys. Res.* 110, <http://dx.doi.org/10.1029/2004jb003501>, B11304.
- Walker, K.T., Bokelmann, G.H.R., Klemperer, S.L., 2004. Shear wave splitting beneath Snake River Plain suggests a mantle upwelling beneath eastern Nevada, USA. *Earth Planet. Sci. Lett.* 222, 529–542.
- Wang, K., Tréhu, A.M., 2016. Some outstanding issues in the study of great megathrust earthquakes—the Cascadia example. *J. Geodyn.* 98, 1–18, <http://dx.doi.org/10.1016/j.jog.2016.03.010>.
- Wells, R., McCaffrey, R., 2016. Steady rotation of the Cascade arc. *Geology* 41, 1027–1030, <http://dx.doi.org/10.1130/G34514.1>.
- West, J.D., Fouch, M.J., Roth, J.B., Elkins-Tanton, L.T., 2009. Vertical mantle flow associated with a lithospheric drip beneath the Great Basin. *Nat. Geosci.* 1, 177–180.
- Xue, M., Allen, R.M., 2006. Origin of the Newberry hotspot track: evidence from shear-wave splitting. *Earth Planet. Sci. Lett.* 244, 315–322.
- Yuan, H., Romanowicz, B., 2010. Depth dependent azimuthal anisotropy in the western US upper mantle. *Earth Planet. Sci. Lett.* 300, 385–394.
- Zandt, G., Humphreys, E., 2008. Toroidal mantle flow through the western U.S. slab window. *Geology* 36, 295–298.
- Zhang, S., Karato, S.-I., 1995. Lattice preferred orientation of olivine aggregates deformed in simple shear. *Nature* 375, 774–777.